NAVAL POSTGRADUATE SCHOOL
Monterey, California

AD-A241 544

DTIC
ELECTE
OCT 2 5 1991
S B D

THESIS

SPATIAL AND TEMPORAL VARIABILITY OF
CROSS-BASIN ACOUSTIC RAY PATHS

by

Coenraad Marinus Ort

December 1990

Thesis Advisor   Ching-Sang Chiu
Co-Advisor   Albert J. Semtner, Jr.
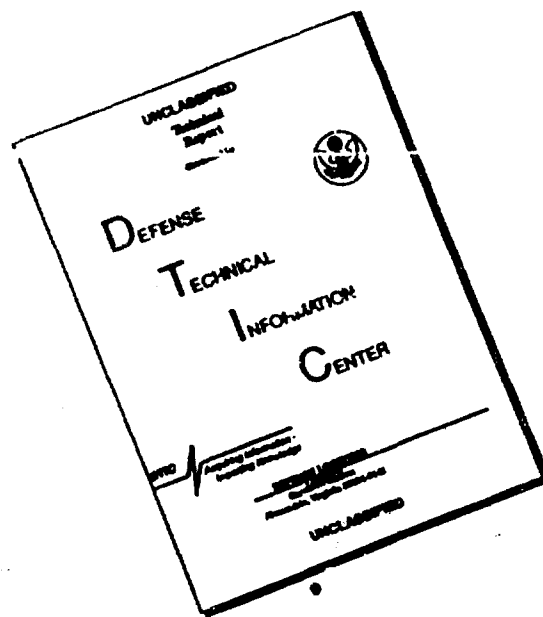
Approved for public release; distribution is unlimited.

91 10 24 159

91-14065

DISCLAIMER NOTICE

THIS DOCUMENT IS BEST QUALITY AVAILABLE. THE COPY FURNISHED TO DTIC CONTAINED A SIGNIFICANT NUMBER OF PAGES WHICH DO NOT REPRODUCE LEGIBLY.

security classification of this page

REPORT DOCUMENTATION PAGE

1a Report Security Classification Unclassified			1b Restrictive Markings				
2a Security Classification Authority			3 Distribution Availability of Report				
2b Declassification Downgrading Schedule			Approved for public release; distribution is unlimited.				
4 Performing Organization Report Number(s)			5 Monitoring Organization Report Number(s)				
6a Name of Performing Organization Naval Postgraduate School		6b Office Symbol (if applicable) 35	7a Name of Monitoring Organization Naval Postgraduate School				
6c Address (city, state, and ZIP code) Monterey, CA 93943-5000			7b Address (city, state, and ZIP code) Monterey, CA 93943-5000				
8a Name of Funding Sponsoring Organization		8b Office Symbol (if applicable)	9 Procurement Instrument Identification Number				
8c Address (city, state, and ZIP code)			10 Source of Funding Numbers				
			Program Element No	Project No	Task No	Work Unit Accession No	

11 Title (include security classification) SPATIAL AND TEMPORAL VARIABILITY OF CROSS-BASIN ACOUSTIC RAY PATHS

12 Personal Author(s) Coenraad Marinus Ort

13a Type of Report Master's Thesis	13b Time Covered From To	14 Date of Report (year, month, day) December 1990	15 Page Count 91

16 Supplementary Notation The views expressed in this thesis are those of the author and do not reflect the official policy or position of the Department of Defense or the U.S. Government.

17 Cosati Codes			18 Subject Terms (continue on reverse if necessary and identify by block number)
Field	Group	Subgroup	Hamiltonian raytracing, greenhouse warming, cross-basin acoustic raytracing

19 Abstract (continue on reverse if necessary and identify by block number)

It was suggested by Munk and Forbes (1989) that climate induced changes in ocean temperature may be monitored by measurements of cross-basin acoustic travel time variability. The feasibility of such a monitoring system depends on the spatial and temporal variability of the cross-basin acoustic paths in the presence of ocean variability of many different scales. For this thesis the variations in arrival position, azimuthal arrival angle, ray trajectory and the corresponding changes in travel times along the three-dimensional multipaths due to meso- and gyre scale ocean temperature fluctuations were analyzed. Emphasis was placed on the acoustic paths from Heard Island in the Indian Ocean, the proposed location for the sound source, to the west coast of the United States.

It was found that the launch angles of reliable, unimpeded acoustic paths to the west coast of the United States lie within a 3° × 2° angular sector. The variability of this ray envelope is discussed.

An optimal receiver site location was found to exist in the vicinity of Monterey Bay, California. The possibility of a proposed listening site location near Coos Bay, Oregon, was also examined. However, the ray paths to Coos Bay interact with the bottom frequently, thus rendering them less reliable.

All the ray traces for this study were carried out using the recently upgraded Hamiltonian raytracing code HARPO, interfaced with output from the Semtner-Chervin eddy resolving global ocean general circulation model. This interface allows for a realistic simulation of the effects of meso- and gyre scale processes on the variability of the various cross-basin paths. The following alternative interfacing methods were investigated: Hardy's multiquadric method and an empirical orthogonal functions method developed by Newhall, et al., 1989.

20 Distribution Availability of Abstract ☒ unclassified unlimited ☐ same as report ☐ DTIC users	21 Abstract Security Classification Unclassified	
22a Name of Responsible Individual Ching-Sang Chiu	22b Telephone (include Area code) (408) 646-3239	22c Office Symbol OC/Ci

DD FORM 1473,84 MAR   83 APR edition may be used until exhausted   security classification of this page
All other editions are obsolete

Spatial and Temporal Variability of Cross-Basin Acoustic Ray Paths

by

Coenraad Marinus Ort
Lieutenant , Royal Netherlands Navy

Submitted in partial fulfillment of the
requirements for the degree of

MASTER OF SCIENCE IN OCEANOGRAPHY

from the

NAVAL POSTGRADUATE SCHOOL
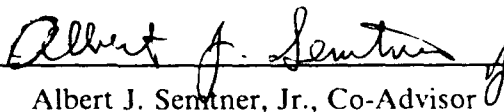December 1990

Author: _____

Coenraad Marinus Ort

Approved by: _____

Ching-Sang Chiu, Thesis Advisor

_____

Albert J. Semtner, Jr., Co-Advisor

_____

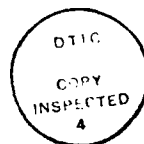Curtis A. Collins, Chairman,
Department Oceanography

ii

ABSTRACT

It was suggested by Munk and Forbes (1989) that climate induced changes in ocean temperature may be monitored by measurements of cross-basin acoustic travel time variability. The feasibility of such a monitoring system depends on the spatial and temporal variability of the cross-basin acoustic paths in the presence of ocean variability of many different scales. For this thesis the variations in arrival position, azimuthal arrival angle, ray trajectory and the corresponding changes in travel times along the three-dimensional multipaths due to meso- and gyre scale ocean temperature fluctuations were analyzed. Emphasis was placed on the acoustic paths from Heard Island in the Indian Ocean, the proposed location for the sound source, to the west coast of the United States.

It was found that the launch angles of reliable, unimpeded acoustic paths to the west coast of the United States lie within a 3° × 2° angular sector. The variability of this ray envelope is discussed.

An optimal receiver site location was found to exist in the vicinity of Monterey Bay, California. The possibility of a proposed listening site location near Coos Bay, Oregon, was also examined. However, the ray paths to Coos Bay interact with the bottom frequently, thus rendering them less reliable.

All the ray traces for this study were carried out using the recently upgraded Hamiltonian raytracing code HARPO, interfaced with output from the Semtner-Chervin eddy resolving global ocean general circulation model. This interface allows for a realistic simulation of the effects of meso- and gyre scale processes on the variability of the various cross-basin paths. The following alternative interfacing methods were investigated: Hardy's multiquadric method and an empirical orthogonal functions method developed by Newhall, *et al.*, 1989.

iii

TABLE OF CONTENTS

ACKNOWLEDGMENTS

This thesis would not be complete without acknowledging several persons who assisted me in conducting the research and presenting my results. First of all I would like to thank Laura Ehret. She guided me through the initially confusing complexity of the HARPO code and offered valuable opinions on many of the problems that were encountered in the course of this study.

Also I would like to thank my co-advisor Professor Semtner for sharing his profound knowledge and insights on numerical ocean modeling and for giving directions in the final writing of this thesis.

Last but not least, I would like to thank Professor Chiu. This thesis could not have been completed in its present form without his assistance. I would like to thank him for inviting me to join his research and for showing me the way to a systematic approach. I have greatly benefited from his guidance and the numerous discussions we have had.

I. INTRODUCTION

A. THE GREENHOUSE EFFECT

Investigation of potential global warming trends, caused by increasing atmospheric content of gases like carbon-dioxide, methane, chlorofluorocarbons (CFC's) and of other trace constituents, is one of the most challenging research topics for this and future decades. Basically, these so called "greenhouse gases" trap heat in the layer between the earth's surface and the level from which radiation escapes back to outer space by absorption of the long wave back radiation from the earth's surface. Increased levels of these gases in the atmosphere will thus raise the earth's temperature, i.e., the "greenhouse effect". Almost everybody agrees on the fact that greenhouse gas concentrations in the atmosphere have increased significantly. Since 1765, levels of atmospheric carbon dioxide have increased from 280 parts per million by volume to more than 350 parts per million. Methane concentration has more than doubled, from 800 to 1700 parts per billion, and nitrous oxide has increased by about ten percent, from 285 to 310 parts per billion. During the past 30 years, concentrations of CFC's have risen from essentially zero to about one part per billion (Jones and Wigley, 1990). However, much controversy exists over related questions concerning the amount of global warming these increases will cause, the time span over which it will take place and whether trends can be discerned and possibly extrapolated to the future. Actual observations of atmospheric surface warming suffer from the fact that many of the land stations are contaminated by significant changes in the micro-climate, especially in urban areas, while sea

1

surface temperature measurements are biased by a conversion from bucket to engine cooling-water intake measurements. Additionally, it is difficult to measure greenhouse warming in the atmosphere, because it has similar spatial patterns as the background air temperature variability. In the ocean the natural temperature variability is significantly different from the expected greenhouse signal. Accordingly, the oceans may be a better environment for early detection of greenhouse warming (Barnett and Schlesinger, 1987).

B. THE HEARD-ISLAND FEASIBILITY EXPERIMENT

It was suggested by Munk and Forbes (1989) that climate induced changes in ocean temperature can be monitored by measurements of cross-basin acoustic travel time variability. The possibility of detection of acoustic transmissions over cross-basin ranges was demonstrated by a 1960 experiment, in which detonations at the depth of the sound channel axis off Perth, Australia, were recorded on hydrophones located near the depth of the sound channel axis in the vicinity of Bermuda (Shockley, et al., 1982). In addition, a *bottom*-mounted hydrophone in the same location also detected significant signal. This result showed that, apart from propagation along the sound channel axis, off-axis cross-basin propagation could also survive and that experimental data could contain information about the temperature field in layers other than only the axial one.

Munk and Forbes (1989) estimated that greenhouse effects warm the sound channel axis at a rate of 0.005 °C per year, which translates into a decrease of acoustic travel time on the order of 0.1 s per year along the cross-basin axial paths. Since meso- and gyre scale processes generate about 1 s rms fluctuations in the cross-basin acoustic travel times,

measurements must le carried out over at least a decade. A field experiment led by the Applied Physics Laboratory in Seattle, Washington, is planned for January 1991 to investigate the feasibility of such a decadal monitoring system. The plan provides for a hydroacoustic low frequency source array to be lowered to about i14 m depth in 1000 m of water southeast of Heard Island (53.2°S / 73.1°E), off Australia in the Indian Ocean. The sources are to be powered from the attending vessel, *R V Cory Chouest*. Initially 12 days of transmissions are planned, cycling through four types of signals: continuous-wave at 57 Hz, a five-tone-like signal called pentaline, a 255 digit maximal-linear-shift register phase-coded sequence, commonly used for tomographic experiments (Spindel, 1985) and longer m-sequences signals. Transmissions will commence on January 24, 1991. The source site near Heard Island was chosen, because it has access to all the major ocean basins. It allows for unimpeded re-fracted ray paths to Bermuda, the west coast of the United States and possibly a path through the Tasman Sea reaching Coos Bay, Oregon, as can be seen in Figure 1.

Investigators from the U.S. Naval Postgraduate School, the Monterey Bay Aquarium Research Institute and the Massachusetts Institute of Technology will jointly deploy a listening array in the vicinity of Monterey Bay on the west coast of the United States.

The feasibility experiment addresses several major uncertainties underlying global acoustic transmissions:

- What is the required source strength for a permanent installation and what type of acoustic source is optimal for this purpose ?

- How is the variability of cross-basin acoustic ray paths affected by spatial ocean variability ?
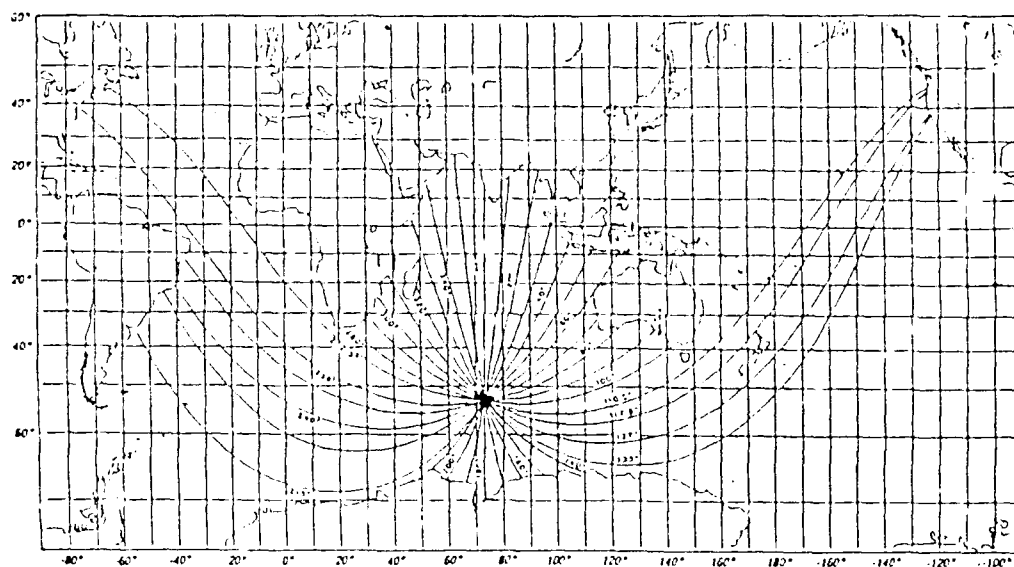
Figure 1. Cross-basin acoustic rays from Heard Island

Source: Munk and Forbes 1989.

- Will the arrival pattern of the acoustic signals have sharp and stable features that allow for determination of the variable travel times with at least 10 ms accuracy ?

- What are the optimal locations for the listening stations and what is the best type of receiver array ?

If the 1991 experiment is successful in demonstrating the feasibility of global acoustic transmissions by resolving these uncertainties, a permanent climate monitoring system could be installed. This permanent system will provide early warning of upper ocean warming in the southern oceans and of interior warming in other oceans.

4

In addition to this possibility of monitoring global ocean warming, a permanent cross-basin range acoustic transmission system could enhance our capability in predicting the ocean's meso- and gyre scale features. Travel time variabili'y along paths going through different ocean basins would contain information on meso- and gyre ale processes in those basins, that can be used for the calibration of eddy resolving global ocean circulation models. The statistics of the measured travel time variability can be used to check the statistics of the global, general ocean circulation model output from time to time for consistency.

C. THESIS OBJECTIVES

This thesis is part of ongoing computer simulation studies of cross-basin acoustic transmissions in support of the analysis and modeling of the field data that will be obtained during the Heard Island feasibility experiment in January 1991. The effects of ocean fronts and eddies on the acoustic ray paths crossing the Indian and Pacific Oceans to the west coast of the United States from a source near Heard Island are investigated. Specifically, the primary objectives of this thesis research are:

- to determine the locations along the west coast of the United States, which will be insonified by the Heard Island sound source;

- to examine and, where possible, quantify spatial and temporal variations in arrival position, azimuthal arrival angle, ray trajectory and the corresponding fluctuations in travel time along the three

dimensional acoustic multipaths, due to meso- and gyre scale ocean temperature fluctuations;

- to investigate whether an optimal listening site location exists in the vicinity of Monterey Bay, California;

- to investigate the potential shadowing effects on the arriving acoustic rays of the shallow "Erben" and "Fieberling" seamounts, located off the California coast;

- to examine the possibility of unimpeded reliable ray paths from the proposed Heard Island source location through the Tasman Sea to Coos Bay, Oregon.

Using numerical models, this thesis attempts to answer some of the crucial questions concerning the usefulness of a global acoustic monitoring system and whether it can be realized. The results presented here will aid in the interpretation and analysis of the experimental data to be obtained in the feasibility field experiment of January 1991. Results will have definite implications for the design of a *permanent* global acoustic transmission experiment, in terms of listening site location, expectable arrival structure, etc..

Naval operations can benefit from this research as well. Results will provide a better understanding of the effects of mesoscale processes on cross-basin low frequency sound propagation in support of naval operations. Western navies have an increasing interest in low frequency long range acoustic prediction research in support of antisubmarine warfare efforts. Low frequency sonar operations, both active and passive, will

benefit from greater knowledge of the characteristics of low frequency three-dimensional wavefields that propagate through oceanic fronts and eddies, while integrated acoustic and physical oceanic modeling capabilities in this field are of prime importance to these operations.

An accurate long range acoustic monitoring and prediction system can only be established through the integration of physical ocean modeling efforts with three-dimensional acoustic modeling. In this thesis the results of such an integration are presented. Prior work in this subject area has only involved the coupling of acoustic models to regional, small domain ocean models (Chiu and Ehret, 1990). The following alternative interpolation methods for the interfacing procedure to link the output data sets from the Semtner-Chervin global ocean general circulation model to the three-dimensional acoustic raytracing model are examined:

- Hardy's multiquadric interpolation scheme (Hardy, 1990) modified for three-dimensional earth-centered spherical coordinates;

- the Empirical Orthogonal Functions (EOF) method, developed by Newhall, *et al.*, 1989.

The comparison between the two methods will aid the continuous effort to examine whether existing procedures and methods in the ongoing acoustic computer simulation studies can be improved in terms of accuracy and efficiency.

D. THESIS APPROACH AND OUTLINE

A three-dimensional Hamiltonian raytracing code, developed originally by Jones, R.M. *et al.* (1986) for a CDC-computer, HARPO, was selected to perform the raytracing in this thesis. Global output data sets, with mesoscale resolution in both space and time, generated by the Semtner-Chervin eddy resolving global ocean general circulation model (1988) were interfaced with the HARPO raytracing code. Simulations were carried out on a UNIX Sun workstation, with a 32 Mbyte random access memory and a 640 Mbyte hard disk memory. In Chapter II the theoretical background of both the ocean- and the acoustic models will be presented. It will contain a discussion on Hamiltonian raytracing and on the global ocean eddy resolving general circulation model. Two alternative methods for the interpolation of the input sound speed fields to the acoustic model from gridded temperature and salinity output data of the Semtner-Chervin ocean model will be discussed in Chapter III. The first method uses spline fits to vertical Empirical Orthogonal Functions (EOF's) and EOF coefficients and has been shown to perform well for small regional data sets (Newhall, *et al.*, 1989). Secondly the performance of Hardy's multiquadric technique, modified for three-dimensional earth-centered spherical coordinates, was tested against observed

8

conductivity, temperature and depth (CTD) data, acquired during the operational oceanography cruise on board *R/V Point Sur* from 5 to 9 May 1990. Based on these tests, the multiquadric technique was rejected and the interfacing procedure, developed by Newhall, *et al.*, (1989), was used for the raytracing simulations.

Raytracing was performed using the HARPO code for a 900-day mean field ocean model output data set, as well as 11 consecutive instantaneous fields, extracted from the model output at 30-day simulation time intervals. Rays were traced from the Heard Island source location, at 1° interval launch azimuth angles and a 2° downward elevation launch angle. All the rays that made it through the Indian Ocean, passing south of New Zealand, and the Pacific Ocean to the west coast of the United States were used in the ray variability analysis. Additionally, the possibility of unimpeded rays through the Tasman Sea, north of New Zealand, was investigated. The results of these analyses are presented in Chapter IV. Variations in arrival position, azimuthal arrival angle, and ray trajectory, as well as the corresponding fluctuations in travel time along the three-dimensional multipaths were estimated. These estimates along with estimates of the locations along the west coast of the United States which will be insonified by the Heard Island sound source and of an optimal

listening site location in the vicinity of Monterey Bay are also presented in this chapter. In Chapter V a summary of this study and its conclusions is presented, along with some recommendations for improving future modeling work of this kind.

II. THEORETICAL BACKGROUND

A. HAMILTONIAN ACOUSTIC RAYTRACING

Many practical problems in ocean acoustics can be solved by applying geometrical acoustics, or ray theory. This technique allows one to simulate the propagation of sound waves through a medium whose refractive index structure varies in a complex manner. The calculations of some acoustic quantities cannot be easily made in any other way, for example, computing multipath pulse travel times or showing which parts of the ocean affect each pulse arrival. However, many raytracing models, which use layers or cells where each raypath segment can be computed in closed form, do not take full advantage of the power of geometrical acoustics. Discontinuous sound velocity gradients at layer interfaces may cause false caustics to occur and cause discontinuous behavior of ray properties as launch angles vary. Often it is also difficult to extend these models to three-dimensional oceans, to account for currents and to compute reflections off complicated bottom topography (Jones, R.M., *et al.*, 1986).

The acoustic model, which is used for this study, is the Hamiltonian Raytracing Program for the Ocean, HARPO. It was designed to overcome the above mentioned limitations. The user defines an ocean model

by writing closed-form expressions for its sound speed and current distribution in three dimensions, and by defining the bathymetry as a function of geographical position. Because it uses continuous models, HARPO avoids the false caustics and discontinuous raypath properties encountered in conventional raytracing methods.

In Hamiltonian raytracing, each raypath is calculated by numerically integrating Hamilton's equations with a different set of initial conditions. These equations are written in terms of a Hamiltonian function, $H(p_1, p_2, \ldots, p_n, q_1, q_2, \ldots, q_n)$, which is the system's total energy (kinetic plus potential), expressed as a function of generalized coordinates $q_1, q_2, \ldots, q_n$, and generalized momenta $p_1, p_2, \ldots, p_n$. Hamilton's equations have the following form:

$$\frac{dp_i}{dt} = -\frac{\partial H}{\partial q_i} \qquad i = 1, 2, \ldots, n. \tag{1}$$

$$\frac{dq_i}{dt} = \frac{\partial H}{\partial p_i} \qquad i = 1, 2, \ldots, n. \tag{2}$$

Lighthill (1987) derived Hamilton's equations for acoustic waves in four dimensions (three spatial and one temporal) for cartesian coordinates, using the "correspondence principle" from quantum mechanics. The

three cartesian coordinates x_i for a "pocket" of wave energy travelling along its ray, correspond to the generalized coordinates q_i in the dynamical system, the wavenumber k_i corresponds to the momentum p_i and the radian wave frequency ω corresponds to the energy H. Lighthill further showed, that ω is constant along rays, which is equivalent to the fact that for any solution of the Hamiltonian equations of motion the total energy H remains constant. This results in the following system of "ray-equations":

$$\frac{dk_i}{dt} = -\frac{\partial \omega}{\partial x_i} \qquad i = 1,2,3. \tag{3}$$

$$\frac{dx_i}{dt} = \frac{\partial \omega}{\partial k_i} \qquad i = 1,2,3. \tag{4}$$

Converting these equations to earth-centered spherical polar coordinates, where r is the radius, ϕ the longitude and θ the co-latitude, gives the following system of six first order equations that are used in the HARPO raytracing code (Jones, R.M., *et al.*, 1986):

$$\frac{dr}{d\tau} = \frac{\partial H}{\partial k_r} \tag{5}$$

13

$$\frac{d\theta}{d\tau} = \frac{1}{r} \frac{\partial H}{\partial k_\theta} \qquad (6)$$

$$\frac{d\phi}{d\tau} = \frac{1}{r \sin \theta} \frac{\partial H}{\partial k_\phi} \qquad (7)$$

$$\frac{dk_r}{d\tau} = -\frac{\partial H}{\partial r} + k_\theta \frac{d\theta}{d\tau} + k_\phi \sin \theta \frac{d\phi}{d\tau} \qquad (8)$$

$$\frac{dk_\theta}{d\tau} = \frac{1}{r} \left(-\frac{\partial H}{\partial \theta} - k_\theta \frac{dr}{d\tau} + k_\phi r \cos \theta \frac{d\phi}{d\tau} \right) \qquad (9)$$

$$\frac{dk_\phi}{d\tau} = \frac{1}{r \sin \theta} \left(-\frac{\partial H}{\partial \phi} - k_\phi \sin \theta \frac{dr}{d\tau} - k_\phi r \cos \theta \frac{d\theta}{d\tau} \right) \qquad (10)$$

Here τ is the independent variable, sometimes proportional to time, whose physical meaning depends on how the Hamiltonian is defined. For acoustic waves in the ocean, the Hamiltonian, which is constant along a raypath, is defined as:

$$H\left(\vec{R}, \vec{k}\right) = \left[\omega - \vec{k}\left(\vec{R}\right) \cdot \vec{V}\left(\vec{R}\right) \right]^2 - c^2\left(\vec{R}\right) k^2\left(\vec{R}\right) = 0 \quad , \qquad (11)$$

where $\vec{V}\left(\vec{R}\right)$ is the ocean current, $c\left(\vec{R}\right)$ is the sound speed field, and ω is the angular wave frequency. $\vec{V}$ and c may also depend on time. Thus, the

14

effects of a three dimensional vector current field are automatically included in the definition of the Hamiltonian.

A few final remarks must be made here about the HARPO code:

- Its computations lie entirely within the scope of geometrical acoustics. It does not apply corrections for diffraction or partial reflections. The ocean model must be deterministic, not random.

- It does not compute acoustic intensity directly. Also, it is not set up to find eigenrays, that connect source and receiver. However, it is relatively straightforward to write supplementary code to carry out these computations.

- It cannot handle refraction at discontinuities of refractive index or its gradients.

- It does not make checks to see if the ocean model satisfies conservation laws and boundary conditions, or that current and sound speed models are geostrophically consistent.

- It integrates the system of Hamiltonian ray equations using the Adams-Moulton predictor-corrector method with a Runga-Kutta starter. Initial conditions are specified in terms of ray launch angles (wavenumber components).

- Since it works in spherical polar coordinates, earth curvature effects are accounted for automatically. However, effects of the earth's ellipticity that cause geodesic veering of the acoustic rays are ignored.

B. THE GLOBAL OCEAN DATA SETS

The continuous ocean model required in the HARPO program is constructed from Semtner-Chervin eddy resolving global ocean general circulation model (SC-model) output data sets. The output of this ocean model was chosen, because it constitutes the only global data set available today, that has mesoscale resolution spatially as well as temporally and

because it has been extensively tested with satisfactory results (Chiu, *et al.*, 1990). The SC-model evolved from the Bryan and Cox model (Bryan and Cox, 1967). Through efforts by several different investigators, this original code was revised to allow for arbitrary bottom topography and coastlines. Also, it was updated for vector-processing and for supercomputers employing multiple parallel processors (Semtner and Chervin, 1988).

The SC-model is a primitive equation, free-thermocline global ocean circulation model. Its domain extends from $75°S$ to $65°N$ and through $360°$ of longitude, with cyclic continuity at $20°E$. It has $1/2° \times 1/2°$ grid spacing in the horizontal and 20 unevenly spaced levels in the vertical. To obtain ocean depths for the model, a data set of global bathymetry available at the National Center for Atmospheric Research for $1/12°$ latitude and longitude points was spatially averaged over $1/2° \times 1/2°$ boxes centered at the model gridpoints. The bathymetry data was smoothed twice, to eliminate topographically induced numerical instability. This procedure resulted in an average ocean model depth of 4400 m and a maximum depth of 5200 m. In addition, some simplifications in geometry were made to create a global $1/2°$ data set of continental outlines. The Arctic was walled off at $65°N$ latitude. The Red Sea, the Gulf of

16

Aden, the Persian Gulf, the Gulf of Oman, the Andaman Sea and the Great Bight of Australia were all filled in. Some major islands were connected to the continental land masses: Madagascar was attached to Africa, the main Indonesian islands were incorporated into a larger, simplified southeast Asian peninsula and the islands of New Guinea and Tasmania were connected to Australia. Other, smaller, islands were replaced with shoals of 100 m depth. This was done, to allow their major topographic features to remain in place, without the need for elaborate, rigorous numerical treatment of these islands. However, the replacement of certain islands by shoals might prove to be troublesome from an *acoustic point of view. Depending on the ray trajectories, acoustic energy* that would otherwise be impeded by these islands, could now possibly leak out through the introduced shoals. Since the ray paths expected in the set up of this analysis will traverse depths that are a lot deeper than 100 m, it is unlikely that this problem will affect the results.

Three "real" islands remained, namely, New Zealand, Australia-New Guinea and Antarctica. The simplified model geometry is presented in Figure 2.
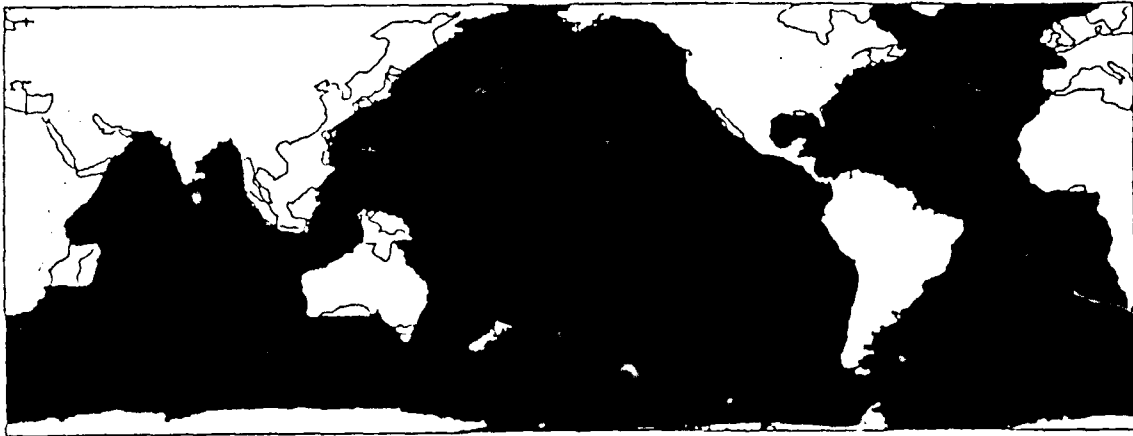
Figure 2.   The Semtner-Chervin global ocean model geometry

Source: Semtner and Chervin, 1988.

In Figure 3 contours of the resulting bathymetry from 500 to 3000 m

for the area of interest in this thesis research are presented. The contour

interval is 500 m, and not all of the geometry simplifications are shown.

It should be noted that two shallow areas exist, that might impede

acoustic rays. The first area south of New Zealand is called the Campbell

Plateau. The second area is the Tasman Sea, between New Zealand and

Australia.   Additionally, there exist two shallow seamounts off the

California coast, that were omitted from the modeled bathymetry. These
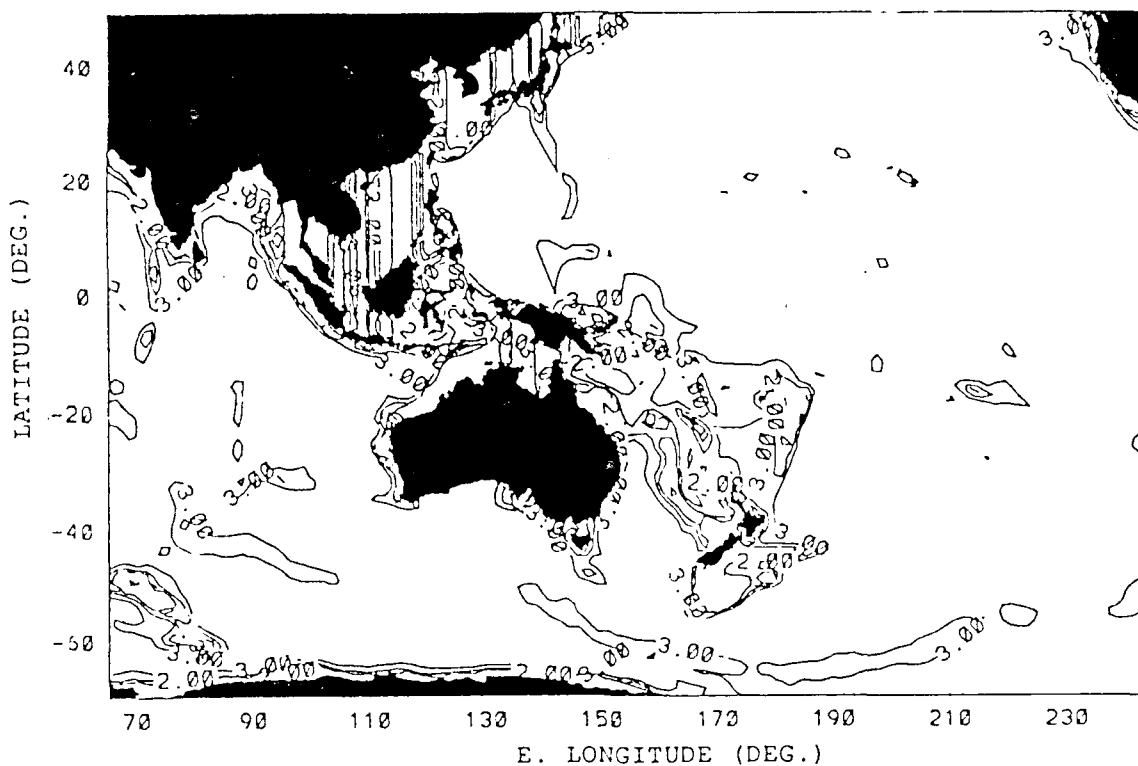
18

Figure 3.   Bathymetry from the Semtner-Chervin ocean model: Contours from 500 to 3000 m, contour interval 500 m.

are: "Fieberling" in position 32.4°N / 23^.7°E, with a depth of 431 m and "Erben" in position 32.9°N / 227.5°E, with a depth of 921 m.   In Chapter IV it will be examined whether the acoustic ray trajectories could possibly be affected by these seamounts.

The 20 vertical levels of the model are unevenly spaced, in a way to give enhanced resolution in the oceanic thermocline, with 12 levels in the upper 1400 m of the water column.   Since acoustic ray paths generally will be confined to depths near the sound channel axis, that normally fall

within the upper 1400 m of the water column as well, the vertical structure of the ocean model will also be adequate from an acoustic point of view. The vertical "boxes" are stacked downward, with the local bathymetry determining the number of boxes. The vertical velocity is defined at the interface between boxes. T, S, u and v are all defined at the same vertical level. T and S are defined at the center of the boxes, while u and v are defined at the midpoints of the vertical edges of the boxes (Long, 1990). This vertical arrangement of grid points is illustrated in Figure 4.

Forcing for the model consists of annual mean wind stress from the Hellerman and Rosenstein (1983) global data sets, interpolated to the $1/2°$ surface velocity gridpoints. A three-dimensional field of temperature (T) and salinity (S) interpolated from the gridded data base of Levitus (1982) is used to force the model at the surface on a monthly time scale and at sub-thermocline depths on a three year time scale. The model was integrated for a simulated time of 22.5 years. Output data were archived at a simulation time interval of three days. With the application of the described forcing method, realistic meso- and gyre scale ocean variabilities resembling many of the observed features in the global ocean resulted from the simulation in the final model years. The mean field output data set, used in this thesis corresponds to a 900-day time average of the data
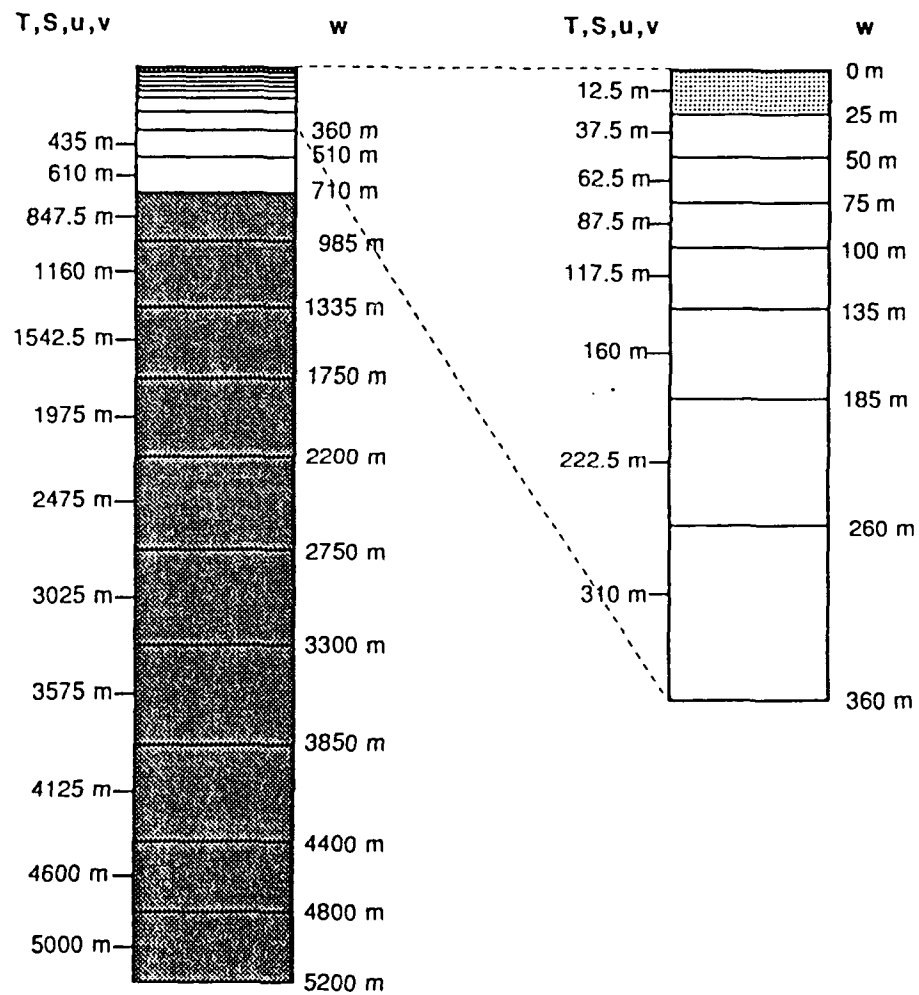
Figure 4.   Vertical arrangement of gridpoints in the Semtner-Chervin ocean model

Source: Long, 1990.

simulated between model years 20 and 22.5. In addition, 11 "monthly" fields, consisting of the instantaneous model output data at a simulation time interval of 30 days, were used to analyze meso- and gyre scale effects on the spatial and temporal acoustic ray variability. In the next chapter the interfacing procedure, which links these data sets to the acoustic Hamiltonian raytracing model, will be discussed.

III. OCEAN-ACOUSTICS INTERFACE

A. INTRODUCTION

The Semtner-Chervin eddy resolving global ocean general circulation model generated approximately 200 Mbyte of data every three simulation days. The data are archived at the National Center for Atmospheric Research. Because the acoustic raytracing simulations were to be carried out on a SUN-4 workstation at the U.S. Naval Postgraduate School, which has only 32 Mbyte of random access memory and a 640 Mbyte hard disk, the task to interface HARPO to the global ocean data set is not a trivial one. To get around this storage problem, two steps are taken (Chiu, *et al.*, 1990):

- Temperature and salinity data in individual ocean basins are first subsampled from the global data set, using a FORTRAN code developed by Altman, 1990. These subsampled data values are then converted to sound speeds using the Mackenzie empirical formula (1981) which has a standard error of 0.070 m/s. Only the subsampled and thus converted sound speed data are transferred to the local SUN-4 workstation.

- The subsampled sound speed data set is still considered large in a workstation environment. Processing all the data at the same time would cause the acoustic computations to come to a virtual halt. To make the simulations tractable, a rectangular window of 10° latitude by 20° longitude is used to move in a discrete fashion with the ray being traced. Only data inside a sub-region with boundaries defined by this window are extracted from the subsampled sound speed data set.

The interfacing procedure furthermore involves the selection of an efficient and relatively optimal interpolator for the generation of continuous sound speed fields, as required by the HARPO code. In this selection process, two different interpolation techniques were examined: 1) Hardy's multiquadric method modified for three-dimensional earth centered spherical, polar coordinates and 2) an empirical orthogonal functions (EOF) method, developed by Newhall, et al., (1989). Both methods will be discussed here.

B. HARDY'S MULTIQUADRIC METHOD

The multiquadric (MQ) method was first discovered in 1968 (Hardy, 1990). It is characterized in two dimensions by the following idea. For each position (x_i, y_i) simply choose a basis function $B_i(x, y)$ and then determine coefficients D_i so that $G(x, y) = \sum_i d_i B_i(x, y)$ interpolates the data (Franke, 1979). The basis function of choice in Hardy's MQ scheme is the upper hyperboloid $B_{ij} = \sqrt{(x_i - x_j)^2 + (y_i - y_j)^2 + \delta^2}$, where δ is a parameter which determines the semi axis of the hyperbolas. Hardy's method can thus be described by the following formula:

$$G(x_i, y_i) = \sum_{j=1}^{n} d_j \sqrt{(x_i - x_j)^2 + (y_i - y_j)^2 + \delta^2} \qquad i = 1,2,...,n \quad (12)$$

Or in matrix notation:

$$G_i = B_{ij}\,d_j \tag{13}$$

The coefficients are found by solving a set of linear equations in terms of the basis functions:

$$d_j = B_{ij}^{-1}\,G_i \tag{14}$$

and the evaluation or prediction (interpolation) at any point p is:

$$G_p = B_{pj}\,B_{ij}^{-1}\,G_i \tag{15}$$

It must be noted, that for $\delta = 0$ the basis function in the interpolation scheme is reduced to a simple measure of distance away from grid points, which diverges linearly with increasing distance. However, non-zero values for δ must be used (even if they are infinitesimally small) to make each term in the scheme infinitely differentiable. For application in HARPO this is a necessary property of the interpolation method to be used. Theoretical investigations have proved that the MQ interpolation is always solvable for distinct data. Franke (1979) performed a critical comparison of about 30 interpolation methods with respect to their capability of reproducing several mathematical surfaces from sparse,

25

scattered data. He concluded after extensive testing, that Hardy's multiquadric method could perform very impressively.

For this investigation the MQ interpolation scheme was modified for application to three-dimensional gridded sound speed data in spherical coordinates. Few people have applied MQ interpolation to more than two dimensions. However, theoretically the method can be applied to any number of dimensions without altering the scheme's basic properties. The basis function in the MQ scheme was transformed in terms of the spherical, polar coordinates r, ϕ and θ:

$B_{ij} = \sqrt{(r_i - r_j)^2 + (\theta_i - \theta_j)^2 + (\phi_i - \phi_j)^2 + \delta^2}$. Equation (12) can now be rewritten as follows:

$$G(r_i, \theta_i, \phi_i) = \sum_{j=1}^{n} d_j \sqrt{(r_i - r_j)^2 + (\theta_i - \theta_j)^2 + (\phi_i - \phi_j)^2 + \delta^2} \quad (16)$$

for i = 1,2,...,n. The coordinates r, ϕ and θ are defined as earth centered spherical, polar coordinates, where r is the radius, ϕ is the longitude and θ is the co-latitude. This modification also allows for easy application of a correction for the earth's ellipticity. One could simply define the local radius, r, as a function of latitude in accordance with a given

26

ellipsoid of choice, using standard geodetic formulas. For cross-basin range acoustic transmissions, this correction is probably not negligible.

To improve the accuracy of the interpolation and to obtain consistent results, the independent coordinates were scaled by dividing the respective terms by appropriate scale parameters. The term involving the radius was scaled by the square of the average ocean depth in kilometers, the longitude term was scaled by the square of the east/west width of the area in radians and the latitude term was scaled by the square of the north/south width of the area in radians. This scaling effectively normalized each of the terms to values between zero and one.

A problem that could be encountered involves so called "track data"; i.e., data points which are closely spaced along one coordinate direction and widely spaced along the two orthogonal directions. Among others, Kansa (1990) found that "track data" give MQ interpolants with very large errors. In our setup we also had to consider "track data", since the unscaled r coordinates have much larger values than the unscaled horizontal coordinates ϕ and θ. However, from existing knowledge of ocean physics it is clear that aside from the uneven spacing of coordinates, we also have to allow for the horizontally stratified nature of the ocean. In effect this causes distinct sound speed values that reside at one and the

same vertical level to be much higher correlated than distinct sound speed values that reside at different vertical levels. To solve for this problem, the normalized integration formula was weighted in such a way, that components in the horizontal ϕ and θ directions seem much smaller than the distance component in the vertical r direction. This assigned a higher "importance" to the sound speed values at grid points that reside at the same vertical level as the position, for which we want to interpolate. At the same time this weighting solved the "track data" problem, as described above. Appropriate values for weighting the terms in the interpolation formula were determined experimentally.

The modified MQ interpolation scheme was tested using data acquired during the operational oceanography cruise, from 5 to 8 May 1990. During this cruise, CTD casts were carried out from the R/V Point Sur at regularly spaced stations in the area between 36.0°-36.7°N and 121.0°-123.0°W, off the California coast. From the CTD data at these stations sound speed values at 20 depth levels were computed from temperature, salinity and depth data, using the Chen and Millero (1977) sound speed formula. This data constituted the "true" observed data. The MQ method was tested by using one part of this data and recovering the other part by interpolation. Interpolation results were examined in

several different experiments. It was observed, that the accuracy of the interpolation results was sensitive to scaling. In general, the results with experimentally determined weighting of the normalized terms performed better than the version of the scheme that was neither normalized nor weighted. The available time for this investigation did not allow for extensive testing of different weighting values. Probably there is room for improvement of the method's accuracy by optimizing the weighting. The mean averaged absolute difference between observed and interpolated sound speed values in the experiments was on the order of 0.5 m/s. This seems like a relatively good preliminary result. However, to detect the expected greenhouse signal, it will be necessary to determine the variable acoustic travel times with at least a 10 ms accuracy (Munk and Forbes, 1989). For the acoustic transmission simulations in this thesis the modified multiquadric scheme would therefore not be sufficiently accurate. The modified MQ scheme performed better, when interpolants were sought at levels that were also used as grid point depth levels. Possibly this is due to the fact, that the additional condition that the sum of the MQ coefficients is equal to zero was not applied here. Effectuating this condition in the algorithm could improve the method's accuracy in future investigations.

The method retrieves grid point data exactly within necessary precision. This reflects the theory behind the method. The size of the area has definite effects on the degree to which the entries in the MQ coefficient matrix are distinct. Kansa (1990) discussed the influence of this distinctness on the goodness of fit of the method. Future research should investigate this matter further. It is suggested to perform testing for larger areas and more vertical levels. Smaller values for δ in general perform better than larger values. The experiments suggested that there exists an optimum value for δ; for this case equal to 10^{-4}. Kansa's suggestion of varying the values of δ with basis function number was not further explored here. Future investigations should not overlook this suggestion. The goodness of fit of the method generally improved when more grid points are used.

The setup and available time for these experiments did not allow for more general and definitive conclusions. The modified multiquadric method seems a potentially useful method for application to global ocean acoustics experiments, especially because corrections for the ellipticity of the earth can be incorporated rather easily. However, apart from this investigation, the method has not yet been used in this field at all and more research is needed. The accuracy of the scheme is, as yet, not sufficient

for application to the global cross-basin range acoustic transmission simulations. It was therefore decided to select the EOF method, which is discussed below. Nevertheless, improvements to the method along the lines suggested could "upgrade" the scheme for actual future use in acoustics projects.

C. EMPIRICAL ORTHOGONAL FUNCTIONS METHOD

In the upgraded version of HARPO, which is used in this thesis, the interfacing method of choice involves the Empirical Orthogonal Fun tions (EOF) representation. In contrast to the experimental nature of the modified multiquadric scheme, the EOF method has been routinely exploited and tested by the physical oceanic community (Newhall, *et al.*, 1989). To begin the description of the EOF scheme, recall how a rectangular window is used to move in a discrete fashion with the ray being traced. Data inside a sub-region with boundaries defined by the window are extracted. Inside this sub-region, sound speed is expressed as a sum of the mean sound speed $\bar{c}(z)$, a function of depth only, and the perturbed speed δc. In formula form:

$$c(\theta, \phi, z) = \bar{c}(z) + \delta c(\theta, \phi, z) \qquad (17)$$

31

The perturbation is then expressed as a linear combination of empirical orthogonal functions (EOF's):

$$\delta c(\theta, \phi, z) = \sum_{i=1}^{N} a_i(\theta, \phi) f_i(z) \qquad (18)$$

where N is at most the number of vertical layers in the ocean model (i.e., 20) , $a_i(\theta, \phi)$ are the horizontal coefficients and $f_i(z)$ are the vertical EOF's. This modal representation has two immediate advantages (Newhall, *et al.*, 1989):

- in representing a three-dimensional function as a product of two-dimensional and one-dimensional functions, one is able to use simple 2-D and 1-D spline routines to supply smooth functions for the field at all points;

- the EOF's are the most efficient energy representation available, so that one needs the fewest number of modes to account for a given percentage of observed variance.

The latter advantage allows one to optimally truncate the mode sum, when the higher modes contain little energy. Preliminary investigations showed, however, that the cross-basin acoustic ray paths are very sensitive to vertical resolution. Ray trajectories change significantly as the number of modes that are retained is changed. Consequently, the maximum number of modes, 20, was used for the analysis presented in this thesis.

32

The next step involves obtaining the mean profile, the EOF's, their coefficients and their energy. A layered mean sound speed profile $\bar{c}(z_k)$ is calculated by averaging all the layered profiles at each horizontal gridpoint within the window, such that the mean at the kth vertical layer is:

$$\bar{c}(z_k) = \frac{1}{M} \sum_{j=1}^{M} c_j(\theta_j, \phi_j, z_k) \tag{19}$$

where M is the number of horizontal gridpoints. In the next step, empirical orthogonal functions of the perturbation profiles are constructed by solving the following eigenvalue / eigenvector problem:

$$\mathbf{A}^T \mathbf{A} \vec{f_i} = \lambda_i \vec{f_i} \tag{20}$$

Thus, the EOF's, $\vec{f_i}$, are the eigenfunctions of the covariance matrix $\mathbf{A}^T\mathbf{A}$ and λ_i are their associated energies. To solve this equation singular value decomposition is used, i.e., set

$$\mathbf{A}^T \mathbf{A} = \mathbf{U}\Lambda\mathbf{V}^T \tag{21}$$

Using this form, the columns of the U matrix are the $\vec{f_i}$ and Λ gives the mode energies. Next, the horizontal coefficients of the EOF's are

33

computed by projecting the layered sound speed perturbation profiles on the layered EOF's, i.e.,

$$a_i(\theta, \phi) = \sum_{n=1}^{N} \delta c(\theta, \phi, z_n) f_i(z_n) \qquad i,n = 1,2,...,N \qquad (22)$$

where i is the mode index and n is the layer index. Cubic splines are then fitted to the mean profile as well as to the EOF's and bi-cubic splines are fitted to the EOF coefficients. This procedure will result in a smooth and continuous sound speed field, as required by the HARPO code.

After the ray is traced to a point near the edge of the window, the window is moved to center at that position. New sub-region data are then extracted and the process is repeated.

IV. ACOUSTIC RAY VARIABILITY ANALYSIS

In this chapter the procedure for and the results of the analysis of acoustic ray variability under the influence of meso- and gyre scale ocean temperature fluctuations are presented and discussed. Emphasis is placed on examining the temporal and spatial variability of the wave front travel times and azimuthal arrival angles of individual rays, as well as the locations along the west coast of the United States being insonified by an envelope of reliable rays launched from a Heard Island sound source and the temporal variability of this ray envelope. The procedure for the analysis along with some results concerning the determination of reliable rays will be discussed first.

A. PROCEDURE

1. Programming Code Modifications

For the ray variability analysis raytracing was performed using the upgraded three-dimensional Hamiltonian raytracing code HARPO. The code was successively interfaced with various output data sets from the Semtner-Chervin global ocean eddy resolving general circulation model, using a empirical orthogonal functions (EOF) method, as described in Chapter III, Section C.

Apart from the modifications involved in the interfacing procedure, two additional changes were be made in the HARPO code. First, the original HARPO output data set did not contain information about the ray point coordinates r, ϕ and θ or the sound speed and sound speed gradient along the ray trajectory. Since such information was necessary for this analysis Ehret (1990) modified the code to produce an extra output data set, i.e., a "rayset", for each HARPO run. containing this supplementary raypath information. In this data set, output values were stored every five integration steps. The rayset-files were subsequently used in all further calculations and processing.

The second change corresponds to approximating the coastline by a straight line in the horizontal plane. This artificial coastline acts as a consistent terminator for the rays. The line was chosen so as to conform as close as possible to the geometry of the Semtner-Chervin ocean model in the vicinity of Monterey Bay, while maintaining its linear character, necessary to simplify the interpretation of the raytracing results. In radians this artificial coastline was defined as:

$$\theta = 1.25 \, \phi - 4.258603376 \tag{23}$$

2. Selecting Reliable Rays

With the modified HARPO code, rays were traced from the Heard Island sound source location using the 900-day mean field ocean model output data set. Subsequently rays were traced using the 11 consecutive instantaneous fields (hereafter to be referred to as the F1 through F11 fields), extracted from the ocean model output data at 30-day simulation time intervals. Because cross-basin rays that encounter frequent bottom interactions suffer significant losses, the corresponding arrivals at listening stations close to the west coast of the United States are unreliable. It is therefore necessary to determine the limiting elevation angles between which the "reliable" rays are confined. A reliable ray is defined here as a ray that is not impeded by land masses and that has fewer than five bottom interactions along its trajectory. To determine the limiting launch elevation angles, rays were traced using a 133° launch azimuth angle in the mean field setup. The launch elevation angle was varied between +4° and -8°, with a 2° interval. It was found that the 0° and -2° launch elevation angles both produced reliable acoustic paths, while the rays with positive or more negative elevation angles invariably became frequently bottom interacting (see for example Figure 5). Since a 0° launch elevation angle requires a nearly infinitely small integration step size in the

raytracing code, which can be troublesome under some circumstances, it was decided to carry out all further raytracing using a 2° downward launch elevation angle, representative of all reliable rays. These reliable rays will probably constitute the latest arrivals, making up the trailing edge of the observed arrival pattern at the receiver. Rays outside the envelope, that interact frequently with the bottom, will generally traverse higher sound speed water and will therefore arrive earlier.

Next, rays were traced with the representative -2° elevation angle and varying launch azimuth angles, to determine the limiting azimuthal angles, between which rays would not be impeded by land masses. For the 900-day mean field ocean model output data set the launch azimuth angles were varied with a half degree increment, while for the F1 through F11 fields an increment of one degree was used. For all fields it was found that only rays within an horizontal envelope between launch azimuth angles of 133° and 136° made it all the way to the west coast of the United States. Rays with smaller launch azimuth angles invariably ran into the Campbell Plateau, south of New Zealand (see Figure 3 on page 19), while rays with launch azimuth angles larger than 136° were impeded by Antarctica. Recapitulating, it was shown that all reliable rays fell within a ray envelope, that was limited vertically by elevation angles
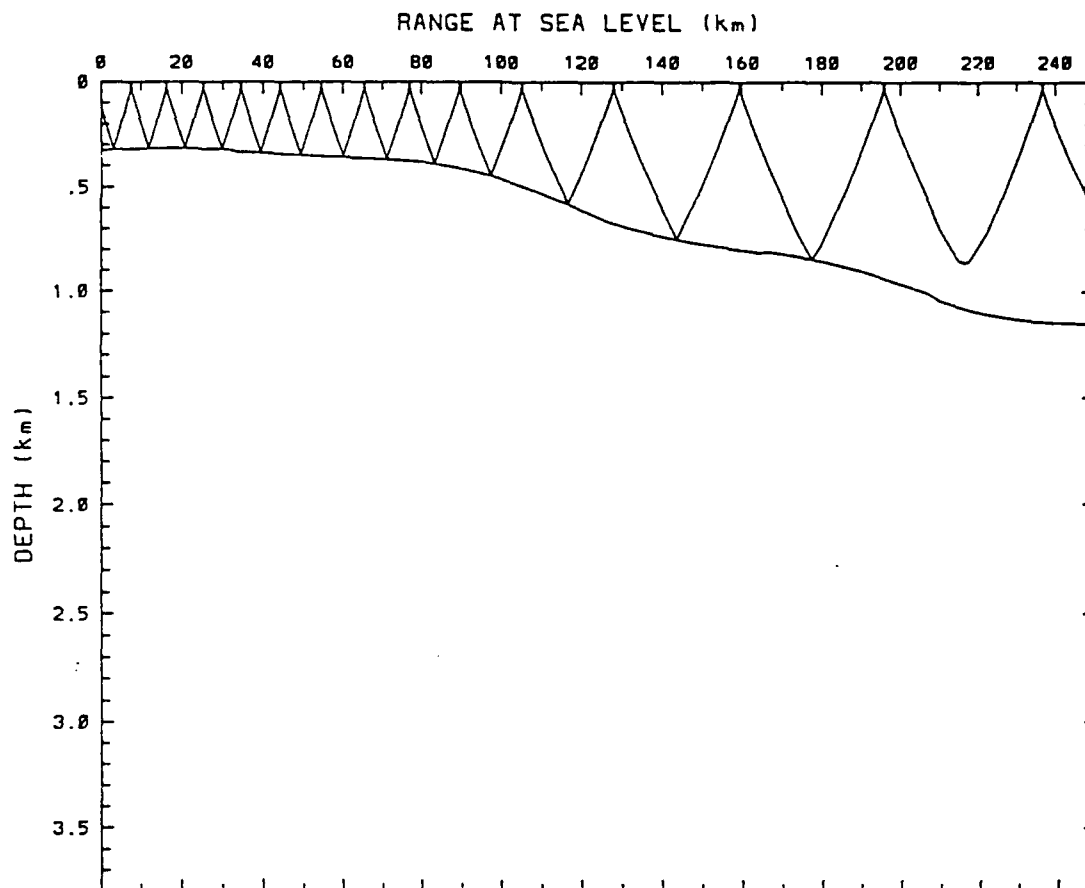
Figure 5. A typical ray path for rays launched with elevation angles smaller than -2°: Vertical section along the ray trajectory for a ray with launch azimuth of 133° and launch elevation of -4°, using 900-day mean field ocean model output data set for a range from 0 to 250 km. This illustrates frequent bottom interactions that rays with elevation angles less than -2° encounter.

of 0° and -2° and horizontally by azimuth angles 133° and 136°. The horizontal trajectories for all reliable rays within this envelope for the mean field are displayed in Figure 6.
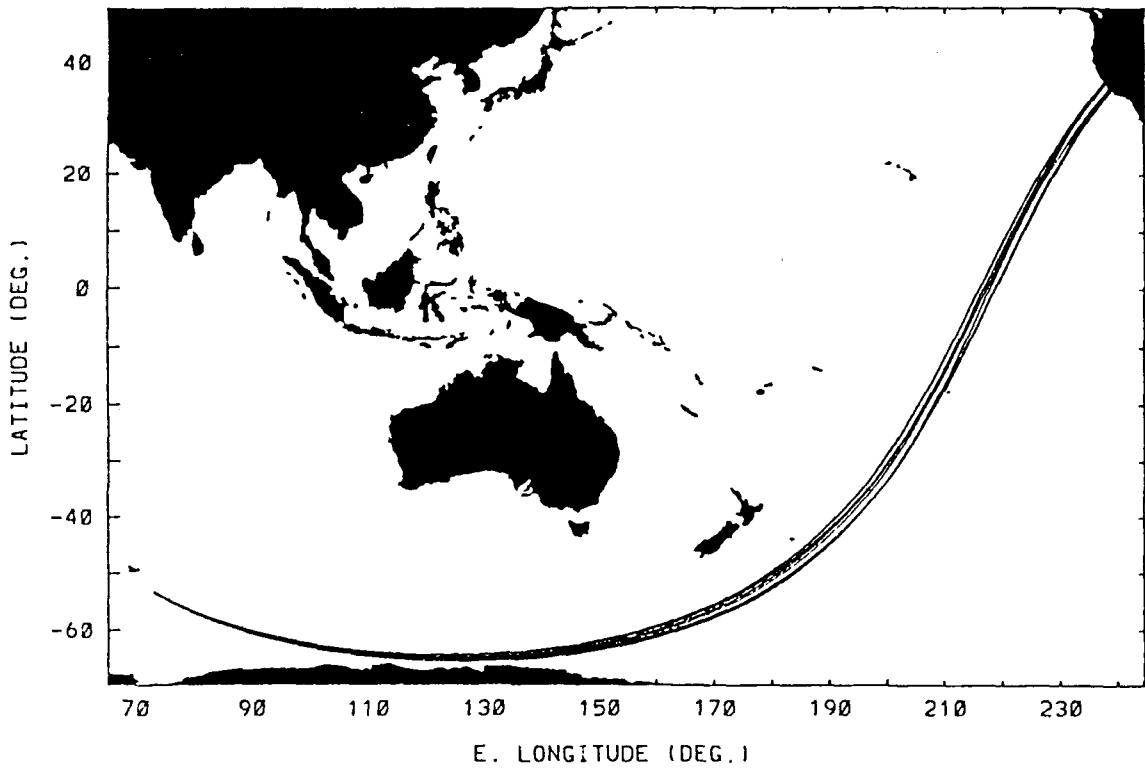
Figure 6. Horizontal trajectories of reliable rays within the ray envelope for the 900-day mean ocean model data field: Rays with the following launch azimuth angles are displayed, from left to right at the source location: 133, 133.5, 134, 134.5, 134.9, 135.5 and 136 degrees.

Although the reliable ray envelopes for all fields were initially the same in terms of limiting launch elevation and azimuth angles, the acoustic paths that define the envelope at ranges away from the source differ from field to field under the influence of the modeled meso- and gyre scale ocean temperature fluctuations.

In the ray variability analysis emphasis was placed on those reliable rays in the described envelope, that made it from the proposed Heard Island sound source location (53.2°S / 73.1°E) through the Indian Ocean, passing south of New Zealand and through the Pacific Ocean to the west coast of the United States. Additionally the possibility of reliable propagation paths from the Heard Island location through the Indian Ocean, the Tasman Sea, *north* of New Zealand and the Pacific Ocean (to Coos Bay, Oregon) was also examined. In this case, using again a 2° downward launch elevation angle in the mean field setup, the azimuthal launch angles were varied between 111° and 119°. It was found that the ray launched with an azimuthal angle of 111° ran into Australia, while the 119° ray was impeded by the northwest coast of New Zealand. All of the rays with azimuthal launch angles in between these limits have excessive bottom interactions in the Tasman Sea, due to its shallow bathymetry and the downward refracting nature of local sound speed profiles. A vertical section along a typical Heard Island to Coos Bay ray trajectory is displayed in Figure 7. No reliable rays could thus be identified for this case.

In carrying out the raytracing simulations it was found that the HARPO code did not handle all rays correctly. In some instances the integration process stopped somewhere along the ray trajectory. Solving
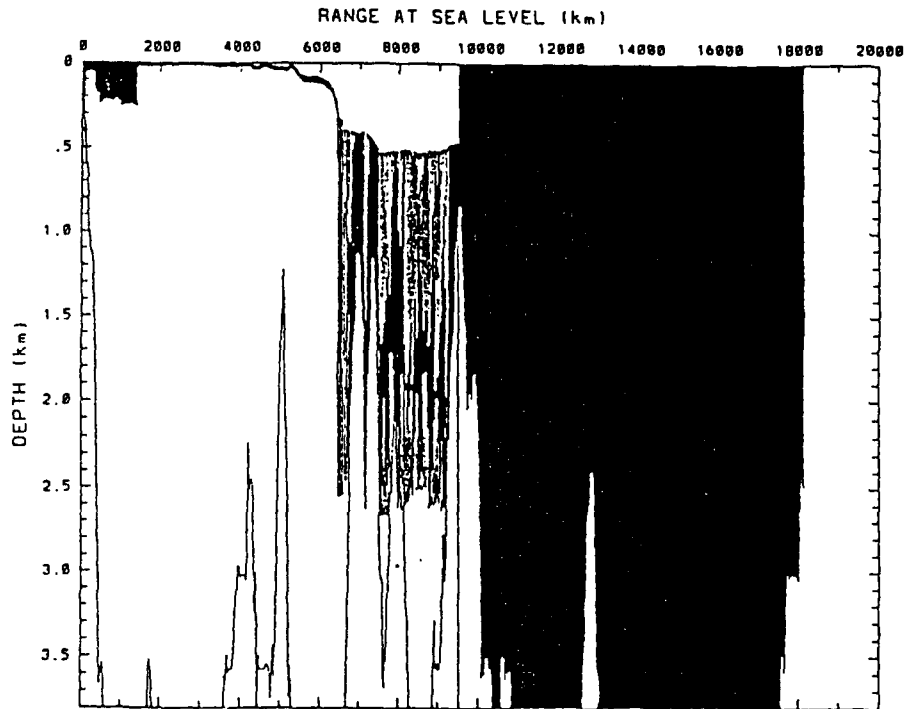
RANGE AT SEA LEVEL (km)

Figure 7.　A typical ray path passing through the Tasman Sea, showing frequent
bottom interaction:　Vertical section along the ray trajectory for a ray
with launch azimuth of 114° and launch elevation of -2°, using the
900-day mean field ocean model output data set and for ranges from 0
to 18000 km.

this programming error is deferred to future investigations.　Whenever a

ray calculation stopped before being finished, the ray was traced again,

using a slight (generally ± 0.1°) deviation from its original azimuthal

launch angle.

For each of the rays traced two plots were produced using NCAR graphics: the first illustrating the horizontal ray trajectory in a cylindrical equidistant projection at the ocean surface; the second depicting a vertical section along the raypath. These plots, in combination with the HARPO output data sets, were studied carefully to determine whether the rays that were traced could be used reliably for the ray variability analysis. All rays that had excessive bottom interactions along their trajectory or were otherwise impeded by land masses, were disregarded and not used any further.

3. Ray Arrival Positions

To find an optimal location for a listening site on the west coast of the United States and to determine whether the shallow Erben and Fieberling seamounts, which were omitted in the modeled bathymetry, could possibly impede the arriving rays, it is necessary to know between what positions reliable rays are expected to arrive. For each selected, reliable ray a stop position on the predefined artificial coastline was computed by direct interpolation between two positions; one on either side of the coastline. The distribution of these arrival positions along the coastline will give a clear indication of the best listening array locations.

4. Wave Front Travel Times

Interpreting the measured arrival pattern of the acoustic signals at the listening site will be greatly facilitated by the results of an analysis of the spatial and temporal variations in acoustic travel times. Travel times to the ray arrival position were directly interpolated from the rayset values. For estimation of wave front travel times to a fixed (receiver) depth, a travel time correction is applied to these values, rather than attempting to find eigenrays, that connect source and receiver.

Whenever a ray does not arrive at the coastline at a depth exactly equal to the receiver depth, the wavefront travel time to a fixed depth will be either shorter or longer than the interpolated ray travel time, depending on the geometry of the particular ray arrival. There are four possible cases: the ray can arrive going upward or downward, at a depth below or above the receiver depth. It is possible to determine the arrival geometry for each ray from the rayset files. From the diagram in Figure 8 it can be seen that the wave front travel time correction is equal to:

$$\Delta t = -\frac{|h\sin(\alpha)|}{c} \tag{24}$$

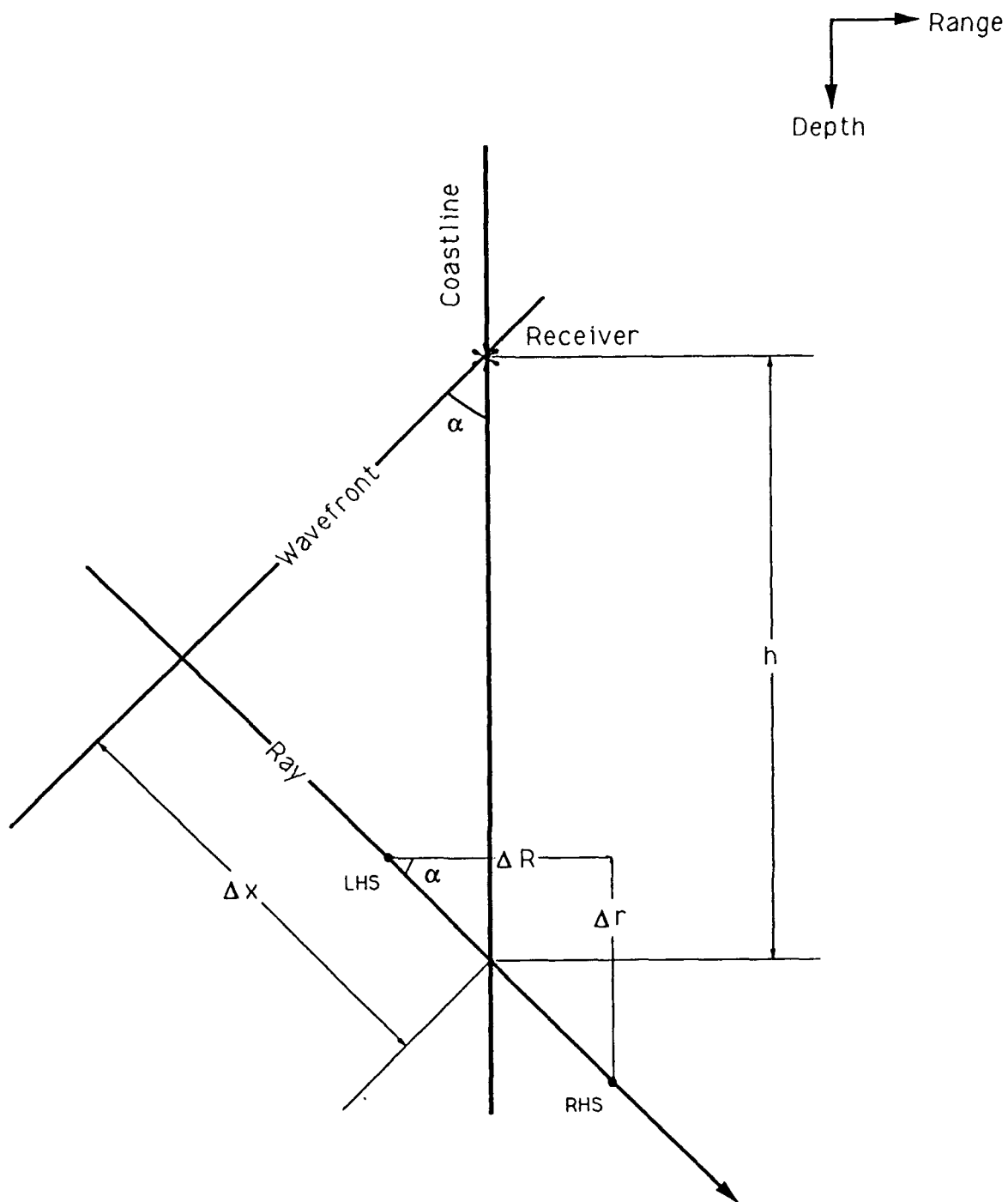where c is the local sound speed.

44

Figure 8. Example of ray arrival geometry for a downward going ray arriving at the coastline below the receiver depth

45

As will be discussed below, the distance between the upper- and lower turning points of the rays, i.e., the ray vertical extent, at ranges larger than about 8000 km turned out to be an important factor in the travel time variability analysis. The double amplitude at a specified range of 12000 km was used for the classification of rays. Two different types of rays were found. This 12000 km range was chosen because, as will be discussed below, it assures that the rays are well away from the transition zone between latitudes 60°S and 40°S, where the largest sound speed variations occur.

5. Azimuthal Arrival Angles

To determine an optimal orientation of a possible horizontal receiver array at the listening site on the west coast of the United States, it is necessary to know angles of the arriving rays and the variability of these angles. For each of the reliable rays the azimuthal arrival angle with respect to north was therefore calculated using standard trigonometric formulas.

B. RESULTS AND DISCUSSION

1. Ray Parameter Variability

Spatial variability of reliable rays within the ray envelopes is attributed to geographical variations in the sound channel axis depth and

sound channel strength. Different rays encounter different transverse and along-path sound speed gradients. Figure 9 displays a contour map of sound speed at the sound channel axis for the 900-day mean field and in Figure 10 the depths of these sound speed minima are contoured[1] .

Rapid fluctuations of the sound channel axis depth and speed occur between latitudes 60°S and 40°S, where the sound speed structure changes f.om a basically upward refracting half-channel regime in the cold Antarctic water towards a deep sound channel regime with an associated shallow surface duct in the more northerly Pacific waters. In this transition zone the sound channel deepens about 800 m in just 10° equatorward, while the axial sound speed increases by more than 20 m/s over the same distance. Since the Heard Island sound source, at 53.2°S / 73.1°E, is located in this transition zone, slight variations in azimuthal launch angle will cause large changes in sound speed along the ray trajectory. Away from the transition zone variations are much more gradual.

In comparing the ray trajectories for the different fields, it was found that a general distinction could be made between two types of rays

---

1 Chiu, *et al.* (1990) found that maps of these two quantities, derived from the Semtner-Chervin ocean model output data used in this analysis, were very similar to those given by Munk and Forbes (1989). This finding fortified the confidence with which this ocean model was used here.
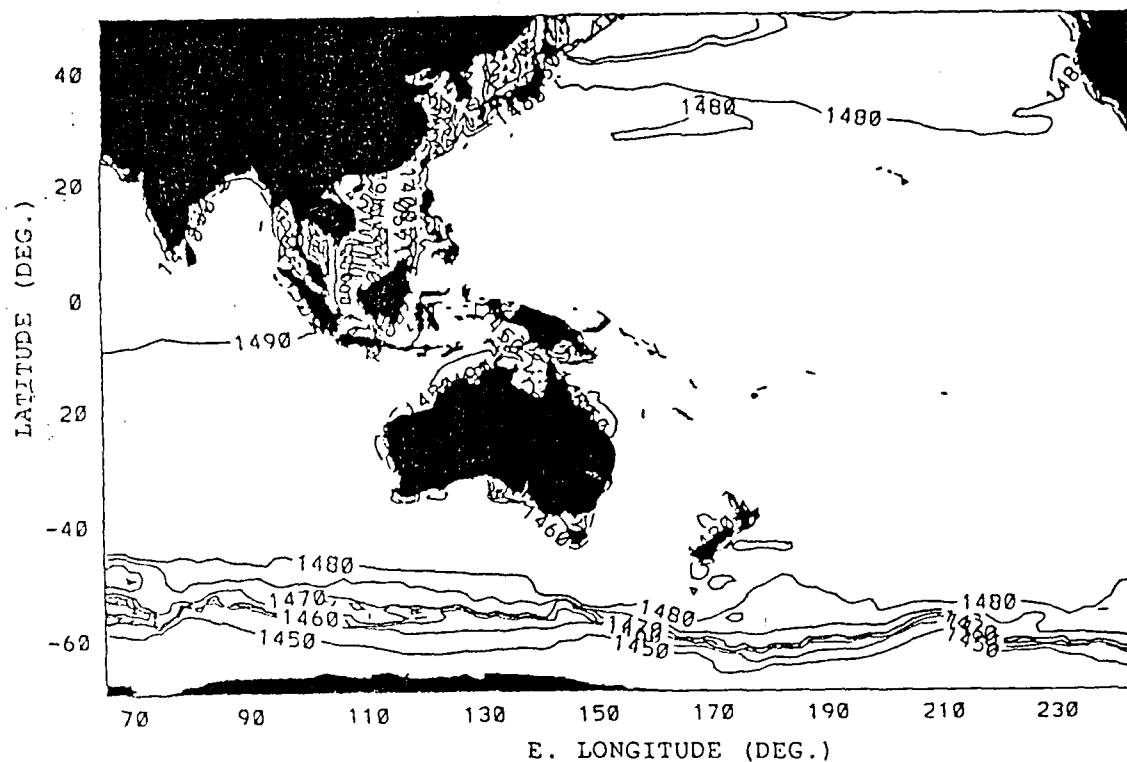
Figure 9.   Sound speed at the sound channel axis for the 900-day mean field ocean

model data set: Contours   from 1450 to 1495 m/s, contour interval

5 m/s.

that were affected in a different way by the modeled sound speed

structure:

- although both types of rays start out in the upward refracting half-channel regime near Heard Island, the first general type of ray (Type I) is trapped closer to the surface than rays of the second type (Type II).   Although the deep sound channel starts to appear at a range of about 5000 km the Type I rays remain trapped close to the surface by the shallow surface duct.   Not until this surface duct weakens between 7500 and 8000 km ranges will the Type I rays enter the deep sound channel.   The distance between the surface duct and
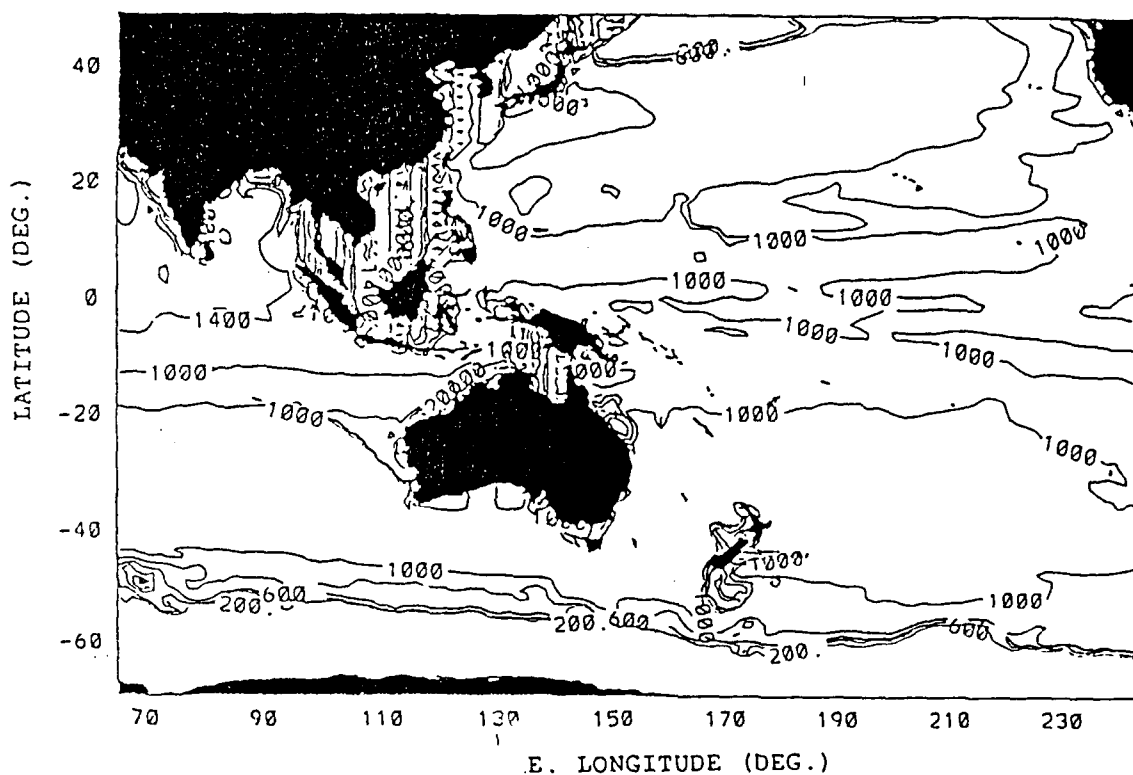
Figure 10.   The depth of the sound channel axis for the 900-day mean field ocean

model data set: Contours   from 200 to 1800 m, contour interval

200 m.

the deep sound channel axis is rather large (about 1200 m), causing the rays to fluctuate about the axis with a large amplitude after the transition.   The wide vertical separation between upper- and lower turning points (generally between 1000 and 2000 m) continues until the ray reaches the west coast of the United States. Since a large part of the ray trajectory traverses high sound speed water on either side of the sound channel axis, the travel times of this type of ray will generally be shorter than those of the second type of ray. Also the Type I rays will encounter larger sound speed variability than Type II rays because the upper parts of the ray trajectories lie within the oceanic thermocline where sound speed variability is largest. Type II rays are confined closer to the sound channel axis, well away

49

from the thermocline and will meet less pronounced sound speed variability.

- the second type of ray is also trapped near the surface in the half-channel regime, but less close than Type I rays. At ranges around 5000 km these rays encounter a stronger along-path sound speed gradient than Type I rays, which forces them to leave the surface duct and enter the deep sound channel below it. Around this range the deep sound channel axis depth gradually increases to about 1000 m over a distance of 600 km. Because of this gradual transition Type II rays will fluctuate about the sound channel axis with a much smaller amplitude than Type I rays. Similar to Type I rays, the distance between upper- and lower turning points (for Type II rays generally less than 500 m) remains almost constant for ranges larger than about 8000 km. Because this type of ray is confined much closer to the sound channel axis, they will traverse lower sound speed water and in general will have longer travel times than rays of Type I. As discussed above, the sound speed variability which these rays encounter along their trajectories will be less pronounced.

All rays fall into either one of these two classifications. Figure 11 displays typical vertical sections along ray trajectories of a Type I and a Type II ray. For completeness, the horizontal trajectories of these rays are illustrated in Figure 12.

In Tables 1 through 5 a summary of the parameters associated with each ray inside the ray envelopes for the various fields is presented. In addition to these tables, variability in ray parameters can be illustrated by means of scatter plots. In such diagrams, the values of certain ray parameters are plotted against arrival latitude along the straight coastline.
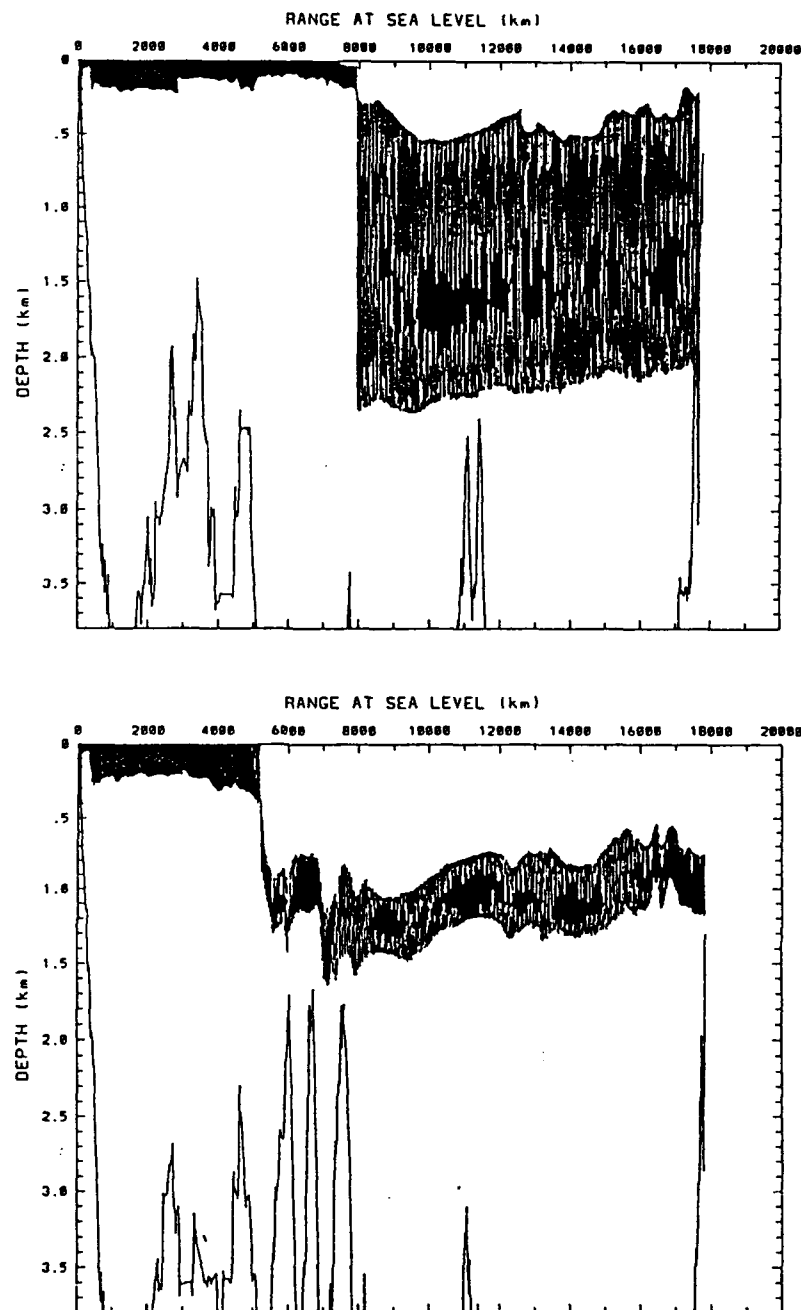
RANGE AT SEA LEVEL (km)

RANGE AT SEA LEVEL (km)

Figure 11. Typical vertical sections along the ray trajectories of a Type I and a Type II ray: Type I ray, launch azimuth angle 135°, F9 field (top); Type II ray, launch azimuth angle 133°, F9 field (bottom). Note that the modeled bottom bathymetry is also displayed.
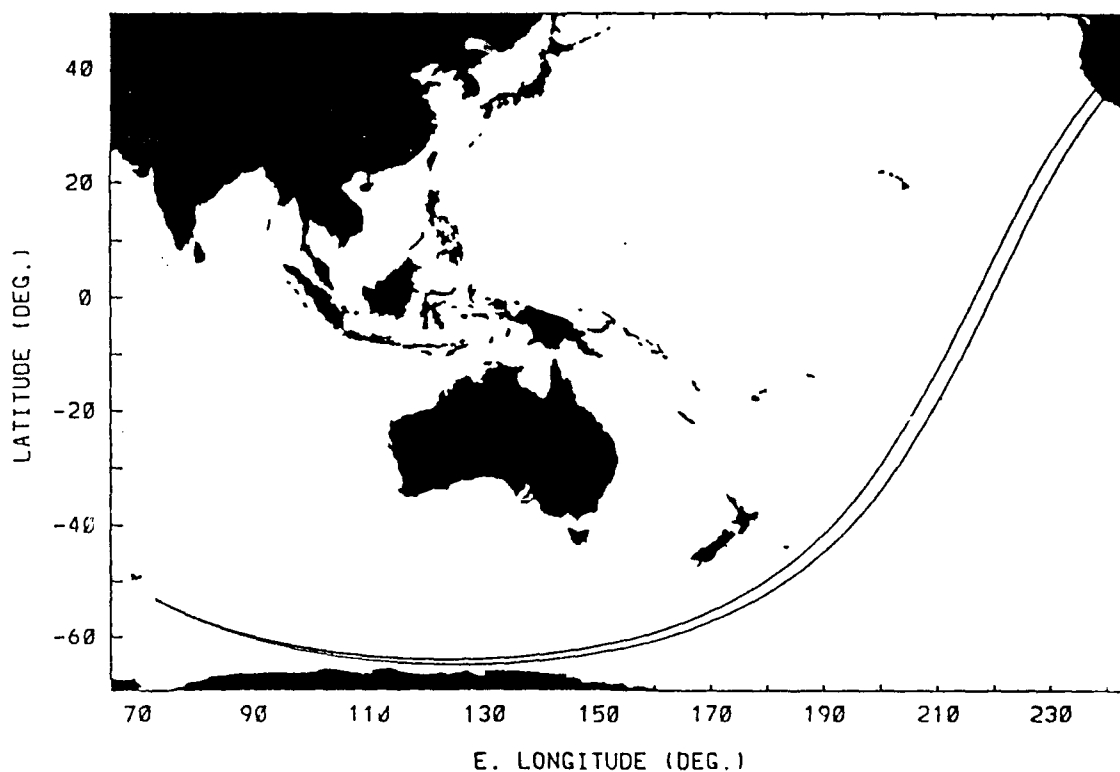
Figure 12.   Horizontal trajectories of typical rays for the F9 instantaneous ocean

model data field: Type I ray with launch azimuth angle 135° on the

right hand side; Type II ·y with launch azimuth angle 133° on the left

hand side.

The scatter plots for wave front travel times and azimuthal arrival angles

are displayed in Figures 13 through 16.

Looking first at the spatial variability in travel times from ray to

ray within the ray envelopes for the 11 instantaneous fields, it can be seen

that the average travel time spread in any of the envelopes is about 62 s.

52

Table 1. MEAN FIELD RAY PARAMETERS

Launch azimuth (deg)	Arrival E. longitude (deg)	Arrival N. latitude (deg)	Arrival angle w.r.t. North (deg)	Wave front travel time (sec)	Ray vertical extent at 12k km range (m)	Type of ray
MEAN FIELD						
132.0	Impeded by Campbell Plateau					
132.5	Impeded by Campbell Plateau					
133.0	237.79	36.77	38.6631	12101.1846	420.0	II
133.5	238.67	35.67	44.9658	12019.6348	1950.0	I
134.0	237.92	36.59	44.9701	12082.7373	440.0	II
134.5	238.08	36.41	36.8631	12079.8018	450.0	II
134.9	239.07	35.16	44.9658	12028.3662	2220.0	I
135.5	238.77	35.53	44.9886	12029.4424	2060.0	I
136.0	237.94	36.57	34.9922	12081.0947	470.0	II
136.5	Frequently bottom interacting near Antarctica					
137.0	Ran into Antarctica					

Table 2. F1-F2 FIELD RAY PARAMETERS

Launch azimuth (deg)	Arrival E. longitude (deg)	Arrival N. latitude (deg)	Arrival angle w.r.t. North (deg)	Wave front travel time (sec)	Ray vertical extent at 12k km range (m)	Type of ray
F1 FIELD						
132.0	Impeded by Campbell Plateau					
133.0	238.19	36.26	39.8179	12078.7139	550.0	II
134.0	238.04	36.46	44.9943	12080.9873	600.0	II
135.0	238.45	35.94	45.0085	12060.8691	500.0	II
136.0	238.01	36.49	35.5488	12072.3945	1000.0	II
137.0	Ran into Antarctica					
F2 FIELD						
132.0	Impeded by Campbell Plateau					
133.0	238.52	35.86	45.0000	12039.7881	2000.0	I
134.0	238.21	36.23	33.7268	12056.3271	1800.0	I
135.0	238.67	35.67	36.8631	12039.8086	1960.0	I
136.0	238.63	35.71	36.2552	12017.5322	1880.0	I
137.0	Ran into Antarctica					

Table 3. F3-F6 FIELD RAY PARAMETERS

Launch azimuth (deg)	Arrival E. longitude (deg)	Arrival N. latitude (deg)	Arrival angle w.r.t. North (deg)	Wave front travel time (sec)	Ray vertical extent at 12k km range (m)	Type of ray
F3 FIELD						
132.0	*Impeded by Campbell Plateau*					
133.0	238.43	35.96	36.8631	12069.2793	300.0	II
134.1	238.17	36.30	44.9943	12049.6924	1790.0	I
135.0	238.61	35.73	36.8631	12041.4619	1880.0	I
136.0	238.04	36.45	45.0341	12053.3643	1900.0	I
137.0	*Ran into Antarctica*					
F4 FIELD						
132.0	*Impeded by Campbell Plateau*					
133.1	238.44	35.96	36.8631	12078.0840	500.0	II
134.0	237.98	36.53	41.1853	12084.0000	290.0	II
135.0	239.00	35.25	36.8631	12021.1396	1820.0	I
136.0	237.58	37.02	33.6927	12109.4238	560.0	II
137.0	*Ran into Antarctica*					
F5 FIELD						
132.0	*Impeded by Campbell Plateau*					
133.5	238.09	36.38	44.9943	12097.1357	590.0	II
134.0	237.97	36.53	45.0043	12089.1748	600.0	II
135.0	239.00	35.25	33.7268	12039.5293	1200.0	I
136.0	237.69	36.90	36.8631	12091.6689	950.0	II
137.0	*Ran into Antarctica*					
F6 FIELD						
132.0	*Impeded by Campbell Plateau*					
133.0	238.21	36.24	36.9068	12074.8457	570.0	II
134.0	237.95	36.57	36.8631	12090.8115	600.0	II
135.0	238.45	35.93	36.8631	12115.6572	1200.0	II
136.0	237.92	36.59	38.6298	12083.0791	950.0	II
137.0	*Ran into Antarctica*					

Table 4. F7-F10 FIELD RAY PARAMETERS

Launch azimuth (deg)	Arrival E. longitude (deg)	Arrival N. latitude (deg)	Arrival angle w.r.t. North (deg)	Wave front travel time (sec)	Ray vertical extent at 12k km range (m)	Type of ray
F7 FIELD						
132.0	*Impeded by Campbell Plateau*					
133.5	238.01	36.48	40.5949	12085.8633	600.0	II
134.0	237.87	36.66	36.8631	12096.8027	400.0	II
135.0	238.43	35.96	35.5229	12067.9502	290.0	II
136.0	237.96	36.55	38.6631	12103.9189	740.0	II
137.0	*Ran into Antarctica*					
F8 FIELD						
132.0	*Impeded by Campbell Plateau*					
133.0	238.16	36.30	36.8631	12092.5117	460.0	II
134.1	238.44	35.96	41.1853	12014.9453	2000.0	I
135.0	238.70	35.62	33.6927	12051.8779	830.0	II
136.0	238.37	36.04	38.6665	12079.1387	510.0	II
137.0	*Ran into Antarctica*					
F9 FIELD						
132.0	*Impeded by Campbell Plateau*					
133.0	238.19	36.27	44.9658	12075.1787	460.0	II
134.1	237.81	36.73	45.0427	12094.2061	490.0	II
135.0	239.55	34.56	44.9943	11984.6299	1810.0	I
136.1	237.97	36.54	38.6665	12093.0654	610.0	II
137.0	*Ran into Antarctica*					
F10 FIELD						
132.0	*Impeded by Campbell Plateau*					
133.0	238.91	35.36	44.9658	12006.6113	1900.0	I
134.0	237.89	36.65	38.6648	12055.5625	1840.0	I
135.0	239.15	35.07	36.8631	12011.4775	1820.0	I
136.0	238.62	35.73	36.8631	12000.8147	2180.0	I
137.0	*Ran into Antarctica*					

55

Table 5. F11 FIELD RAY PARAMETERS

Launch azimuth (deg)	Arrival E. longitude (deg)	Arrival N. latitude (deg)	Arrival angle w.r.t. North (deg)	Wave front travel time (sec)	Ray vertical extent at 12k km range (m)	Type of ray
FI1 FIELD						
132.0	Impeded by Campbell Plateau					
133.0	239.40	34.74	41.6392	11964.6611	2200.0	I
134.0	238.55	35.81	39.2828	12010.5859	1920.0	I
135.1	239.31	34.86	36.8849	12005.1914	1860.0	I
135.9	238.16	36.30	44.9886	12096.1309	620.0	II
137.0	Ran into Antarctica					

The maximum wave front travel time spread is 131.5 s in the F11 field envelope and a minimum spread of 20.1 s is found in the ray envelope of the F1 field. The distinction between the Type I and Type II ray travel times is confirmed in Figure 14. The Type I rays generally have shorter travel times than the Type II rays. The travel times of the two groups have little overlap.

Apart from this spatial variability, the wave front travel times also exhibit fluctuations that are due to variability of meso- and gyre scale ocean processes in time. A rough estimate of the temporal variability in travel time can be obtained by examining the travel time values found along lines of constant latitude. The scattered travel time values at a given latitude are an indication of the temporal rms fluctuations from field to field. A visual estimate of the rms temporal wave front travel time
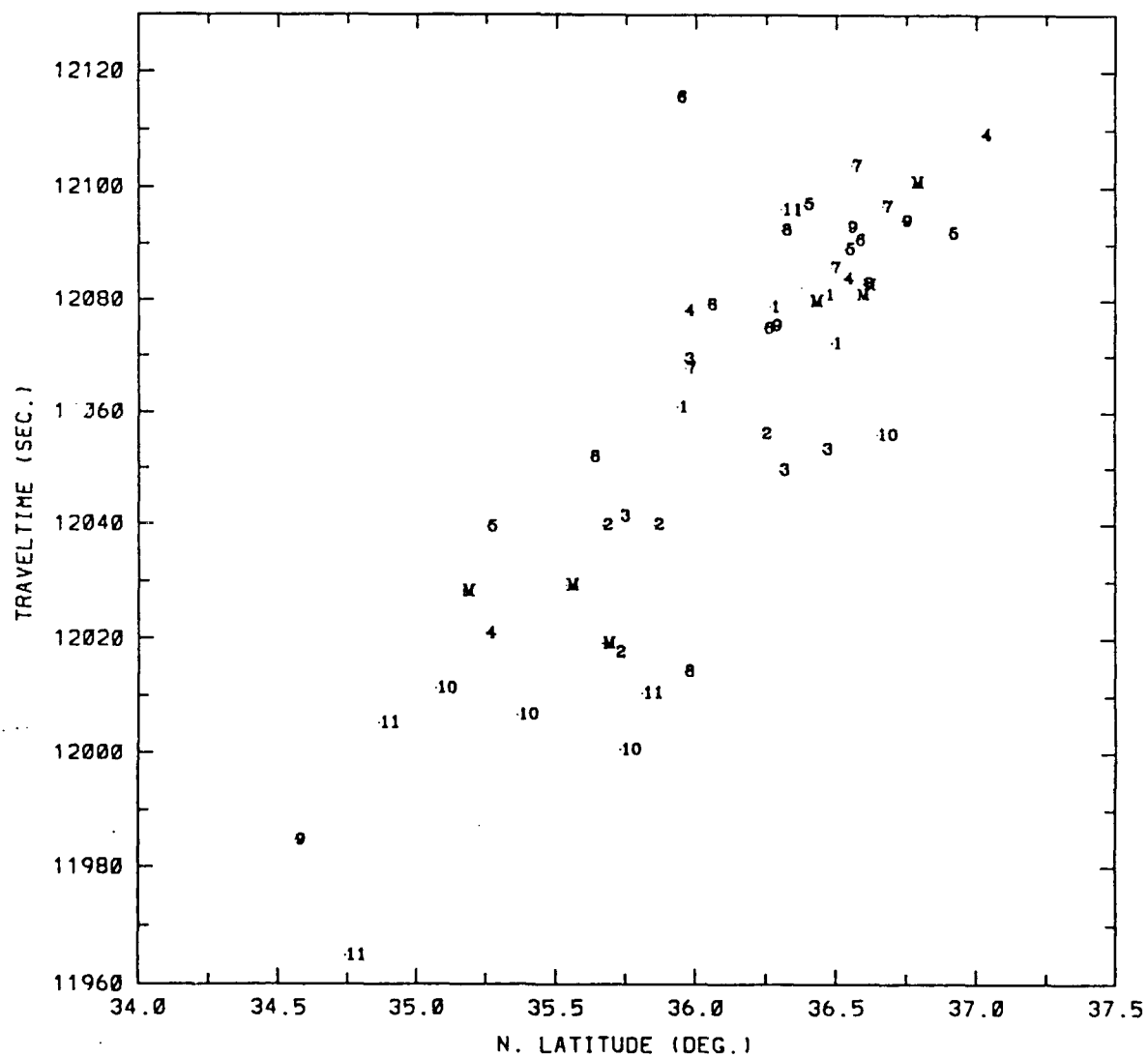
Figure 13. Wave front travel time scatter plot as a function of latitude, showing the distinction between different fields: Travel times labeled with M are for mean field rays, labels 1-11 are for the F1-F11 fields respectively.
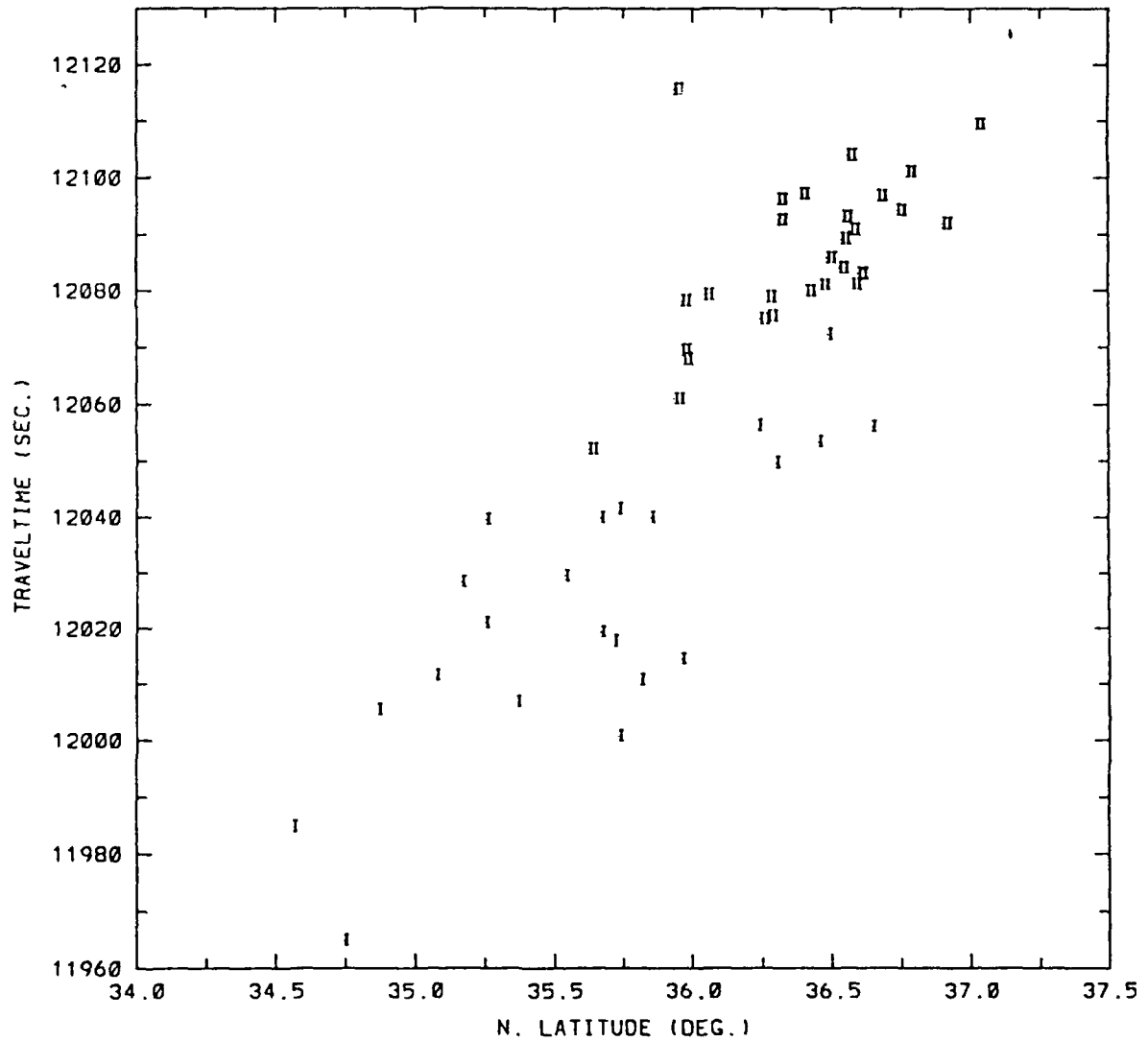
57

Figure 14. Wave front travel time scatter plot as a function of latitude, showing the distinction between Type I and Type II rays: Travel times labeled with I are for Type I rays, label II applies to Type II rays.
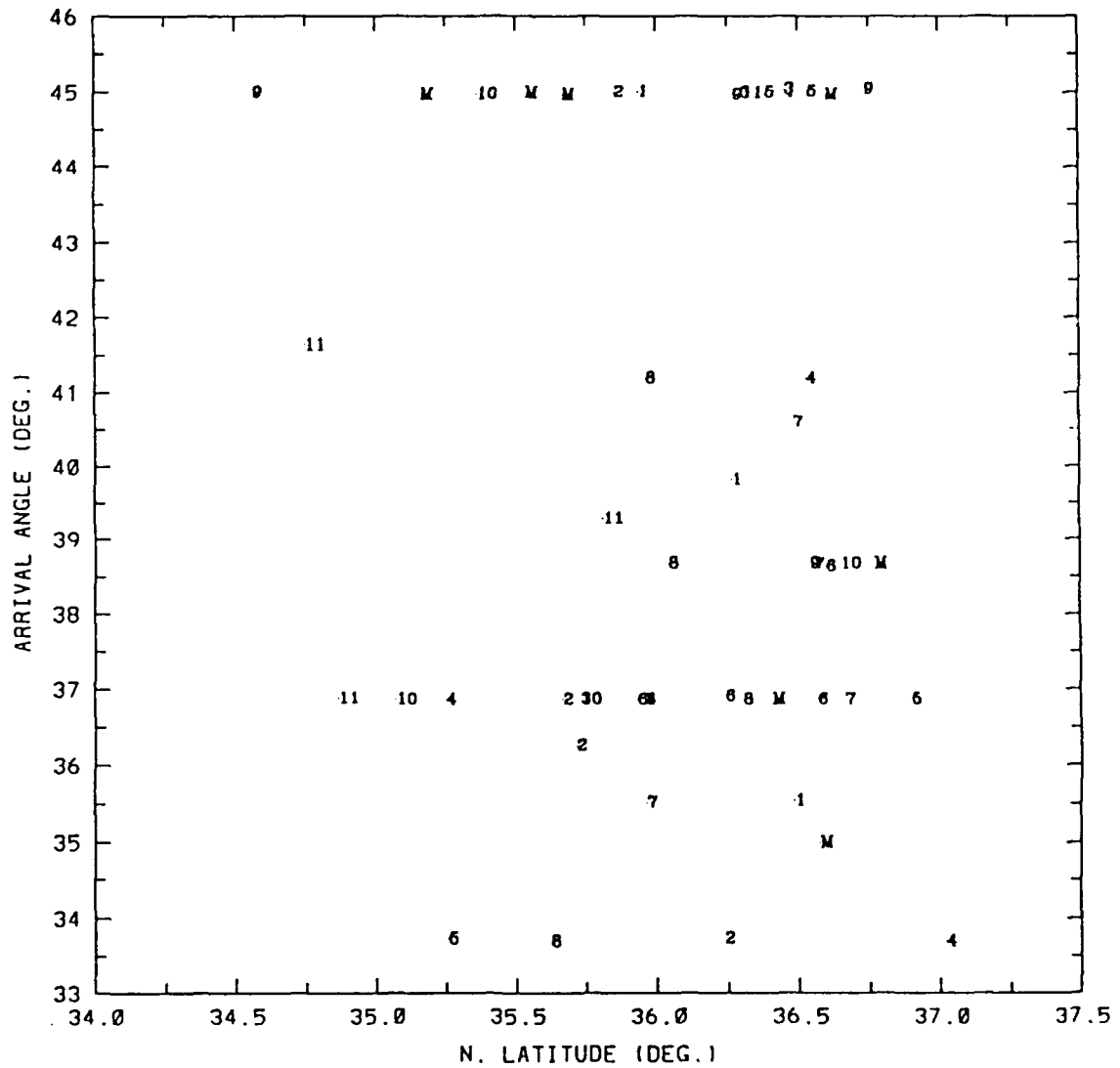
Figure 15. Azimuthal arrival angle scatter plot as a function of latitude, showing the distinction between different fields: Arrival angles labeled with M are for mean field rays, labels 1-11 are for the F1-F11 fields respectively.
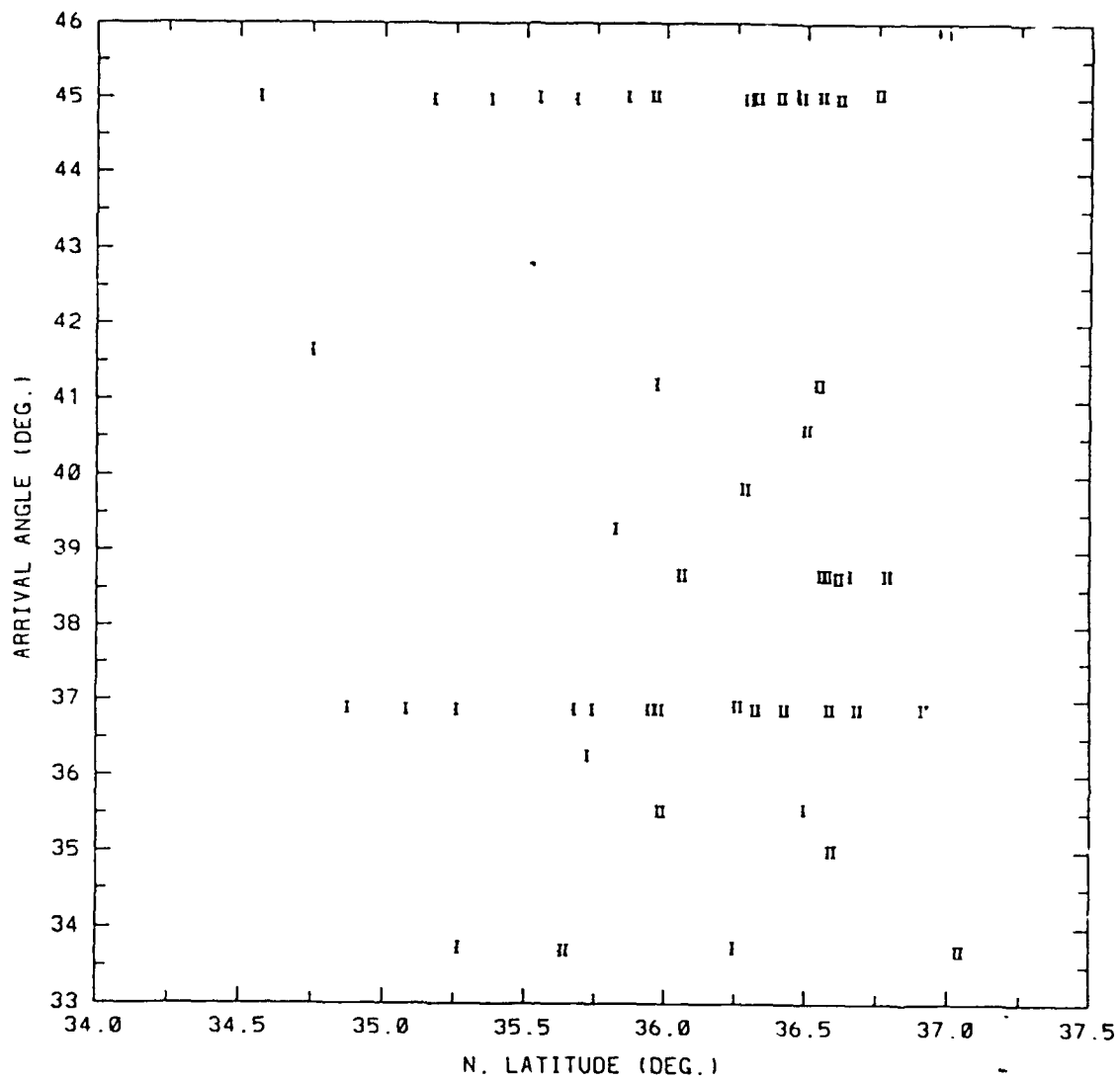
Figure 16. Azimuthal arrival angle scatter plot as a function of latitude, showing the distinction between Type I and Type II rays: Arrival angles labeled with I are for Type I rays, label II applies to Type II rays.

variability is on the order of $\pm$ 15 s. Comparing the travel times for the Type I and Type II rays in Figure 14, it is clear that the temporal rms fluctuations in this ray parameter for the Type II rays (about $\pm$ 10 s), is almost twice as small as the rms fluctuations for the Type I rays (about $\pm$ 20 s). Apparently the temporal variability is larger for rays that traverse larger distances away from the sound channel axis, i.e., the Type I rays. This is due to the large temporal sound speed variability in the oceanic thermocline, which is traversed by the Type I rays only. The variability along the sound channel axis, where the Type II rays are confined is smaller.

In a recent investigation Semtner and Chervin (1990) quantified the temporal meso- and gyre scale effects, as well as seasonal effects, on acoustic travel times along three stationary axial acoustic paths. They found that the travel time to San F anc sco fluctuates about 0.5 s around a 360-day running mean[2] under the influence of mesoscale ocean variability. One of their conclusions, based on these findings, states that the mesoscale effects on acoustic travel times are not large enough to obscure the anticipated signal of global change in the ocean. However, in their analysis they ignored path changes induced by the ocean variability.

---

2 It should be noted that the interval at which data were extracted from the ocean model output in the Semtner-Chervin investigation was 3 simulation days, compared to the 30-day simulation time interval between the F1 through F11 fields used in this thesis

Comparing their results with the results presented above, it is obvious that the temporal wave front travel time fluctuations found in this thesis are at least one order of magnitude larger than the ones found by Semtner and Chervin. Apparently the additional effects of path changes that were simulated in this thesis, but were not considered by Semtner and Chervin, are not negligible. Whether these additional effects due to changes in the acoustic paths are so random that they can be averaged out to allow for the detection of a greenhouse signal, cannot be answered within the scope of this thesis. Future investigations using more samples should address this problem.

Next, the variability in azimuthal arrival angles is examined in an analogous manner. An indication of the spatial variability is obtained by looking at the spread between extreme values inside the different ray envelopes. On the average this spread is about 8.0°. A maximum occurs in the F5 field envelope with 11.3°, while the minimum of 1.8° is found inside the ray envelope of the F6 field. The temporal rms variability is estimated from the scatter diagrams in Figure 15 and Figure 16. It can be seen that this rms variability has an approximate magnitude of ± 4.0°. These figures illustrate how most arrival angles are concentrated around values of 37° and 45°. Unlike the effects on travel times, no clear

cut distinction between the spatial and temporal effects on azimuthal arrival angles of Type I rays and on those of Type II rays could be made.

Looking at the scatter plots that show the distinction between Type I and Type II rays, it is evident that Type I rays generally arrive more to the south on the coastline than the Type II rays. This is due to the fact that rays of Type I traverse a much larger part of the water column than rays of Type II. Consequently, they will accumulate more southward horizontal refraction while crossing the circumpolar frontal system.

2. Insonification Area and Envelope Variability

Apart from the analysis of the parameters of individual rays, such as wave front travel times and azimuthal arrival angles, it is also necessary to define, compute and analyze quantities that describe the ray envelope which insonifies the California coast. The mean of the arrival positions of the rays within an envelope is an estimate of the location on which the sound energy is focused, i.e., the *envelope focus*. The standard deviation of these arrival positions is a relative measure of how much the rays inside the envelope diverge away from the position of this focal point. A smaller *envelope divergence* (i.e., the standard deviation) implies a stronger envelope focus. The *envelope width* is defined as the width of the area which

is insonified by a particular ray envelope. The *envelope center* is the center of the insonified area. In Table 6 below, an overview of these envelope parameters is presented.

Table 6. RAY ENVELOPE PARAMETERS

Field	Envelope focus longitude (deg)	Envelope focus N. latitude (deg)	Envelope center longitude (deg)	Envelope center N. latitude (deg)	Envelope divergence (km)	Envelope width (km)
F1	238.17	36.29	238.23	36.21	29.0	72.6
F2	238.51	35.87	238.44	35.95	29.5	75.1
F3	238.31	36.11	238.33	36.09	37.3	95.3
F4	238.25	36.19	238.29	36.13	87.1	233.9
F5	238.19	36.27	238.34	36.08	81.1	217.2
F6	238.13	36.33	238.19	36.26	35.8	87.8
F7	238.07	36.42	238.15	36.31	35.4	92.2
F8	238.42	35.98	238.43	35.96	32.2	90.0
F9	238.38	36.02	238.68	35.65	113.8	287.1
F10	238.64	35.70	238.52	35.86	78.4	208.5
F11	238.86	35.43	238.78	35.52	86.3	206.6
Average	238.36	36.06	238.40	36.00	58.7	151.5
St. dev.	0.23	0.28	0.19	0.24	29.3	75.3

Clearly the results in Table 6 illustrate which area along the California coast is insonified by the Heard Island sound source, as well as the temporal variability of the insonification envelope. Considering all 11 envelopes, it can be seen that the focus positions fluctuate around an average longitude of 238.36°E and an average latitude of 36.06°N, with a standard deviation in longitude of about 0.23° and in latitude of about 0.28°. The centers of individual ray envelopes vary around a mean

longitude of 238.40°E and a mean latitude of 36.00°N, with slightly smaller standard deviations of 0.19° and 0.24° respectively. The focal points for the individual envelopes are invariably different from the envelope centers and can be located on either side of these centers. The average distance between focus and centers is 15.2 km, a maximum of 50.1 km is found for the F9 envelope and a minimum of 2.4 km for the F8 envelope. The strength of the foci, as expressed by the envelope divergences, varies largely. The maximum divergence is 113.8 km, the minimum is 29.0 km and the standard deviation over all envelopes is 29.3 km. The width of the area along the California coast that is insonified by the individual envelopes varies from 72.6 km for the F1 field to 287.1 km for the envelope in the F9 field. The mean width is 151.5 km with a standard deviation of 75.3 km. Generally, a larger envelope width will imply a larger envelope divergence.

C. THE 1991 FEASIBILITY EXPERIMENT

The last section in this chapter is devoted to translating the above findings to practical implications for the planned 1991 feasibility experiment. The simulations and subsequent analysis in this thesis demonstrated the existence of unimpeded reliable acoustic path cross-basin range ray trajectories from the Heard Island sound source location to the

west coast of the United States. It was found that reliable rays fall inside a 3° × 2° angular sector bounded by launch azimuth angles of 133° and 136° and launch elevation angles of 0° and -2°. Rays launched outside this angular sector will be impeded by the Campbell Plateau, south of New Zealand, or Antarctica, or will interact with the bottom frequently, thus rendering them unreliable.

The expected positions of ray arrivals in the vicinity of Monterey Bay were shown to fluctuate between 34.56°N / 239.55°E and 37.02°N / 237.58°E, with a mean focal point at 36.06°N / 238.36°E. A permanent Monterey Bay listening station should optimally be located near this position. A ship that deploys a listening array during the 1991 feasibility experiment should provide experimental verification of this finding.

Figure 17 illustrates the area of insonification and acoustic path density for all simulated rays in the F1 through F11 fields. From this figure it can be seen that the arriving rays stay well clear of the shallow Fieberling seamount, in position 32.4°N / 232.2°E. The other seamount, Erben, in position 32.9°N / 227.5°E falls outside of the plot boundaries and is also located well away from the envelope of arriving rays. Both

seamounts are thus expected to have no impeding effect on the ray arrivals in the vicinity of Monterey Bay.

The possibility of reliable ray paths to Coos Bay, Oregon, was shown to be very slim. Rays within a azimuthal launch angle envelope between 111° and 119° invariably interacted excessively with the shallow bathymetry in the Tasman Sea. It will probably be very difficult to detect the corresponding lower energy arrivals at a listening site near the Oregon coast.

The wave front travel time that can be expected is approximately 12060 s, with a variation of about 20 to 131 s. Most probably the reliable rays will constitute the latest arrivals, making up the trailing edge of the observed incoming acoustic arrival pattern. Estimated temporal rms fluctuations of the trailing edge at the receiver are on the order of $\pm$ 15 s.

Finally, it must be noted that the analysis did not allow for geodesic veering of acoustic rays under the influence of the earth's ellipticity. The HARPO code worked in polar, spherical coordinates and no ellipticity corrections were applied. To find an initial estimate of the magnitude of the error introduced by this omission, great-circle as well as geodesic trajectories were calculated using programs obtained from the National
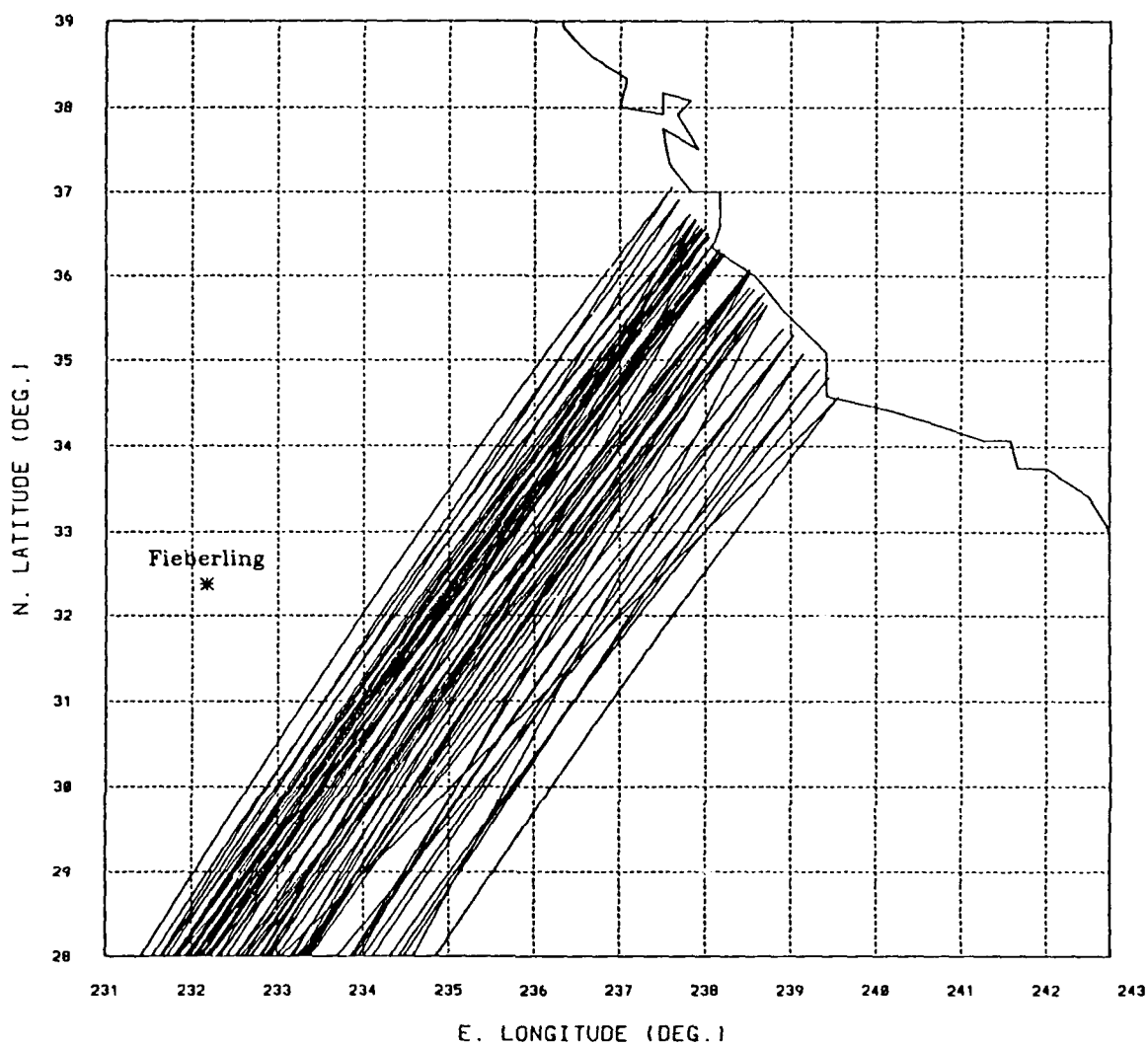
Figure 17.   Area of insonification and acoustic path density in the vicinity of Monterey Bay: All ray arrivals for the F1 through F11 fields are shown. Position of Fieberling seamount is marked with an asterisk; Erben seamount in position 32.9°N / 227.5°E, falls outside of the chart boundaries.

Oceanic and Atmospheric Administration[3]. In Figure 18 portions of great-circle and geodesic paths in the vicinity of Monterey Bay are displayed. These non-acoustic paths have initial azimuth angles of 133, 134, 135 and 136 degrees at the proposed Heard Island source location. From this plot it can be seen, that the geodesic paths always arrive more to the north than the great-circle trajectories. The distance between arrival positions near the coast is on the order of 22 km. Based on this finding, it is expected that acoustic ray arrivals in reality will deviate to the north from their arrival positions presented in this thesis by about that distance, due to geodesic veering. Also it can be seen that the non-acoustic geodesic and great-circle paths are impeded by the shallow Fieberling seamount. However, acoustic rays are affected by large sound speed gradients in the transition zone, resulting in a southward displacement of about 350 km. As was shown above, this displacement due to horizontal refraction is large enough for the acoustic rays to stay well clear of the seamount.

---

[3] It must be emphasized, that the trajectories computed in this manner do not represent acoustic ray paths, but are the mere results of applying standard geodetic formulas.
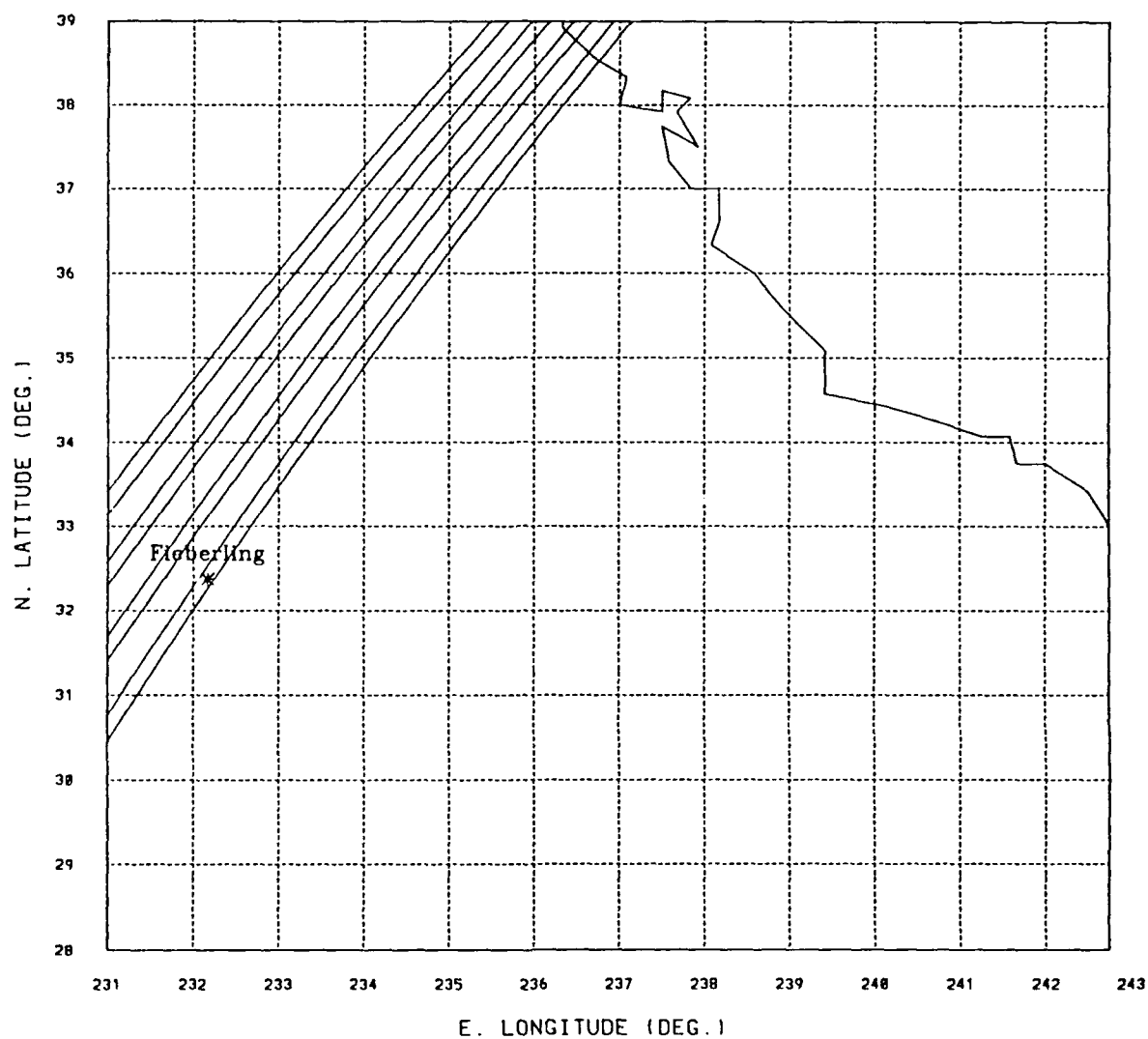
Figure 18. Great-circle and geodesic paths near Monterey Bay: Initial azimuth angles at the Heard Island source location were 133, 134, 135 and 136 degrees, from bottom to top. In each pair of paths the geodesic is located to the north of the great-circle path.

V. CONCLUSIONS

In this final chapter the results and conclusions of this study will be summarized. Some final remarks along with recommendations for future work will also be made.

A. SUMMARY OF RESULTS

1. Reliable Rays

In this study reliable rays were defined as rays that have less than five bottom interactions along their trajectories and that are not impeded by land masses. It was shown that all reliable rays will be confined to a ray envelope, bounded by launch elevation angles of $0°$ and $-2°$ and azimuthal launch angles of $133°$ and $136°$. The envelope dimensions are invariant in time near the source, but can be quite variable at the California coastline.

2. Area of Insonification and Optimal Receiver Site Location

One of the primary objectives of this study was to determine the locations along the west coast of the United States that will be insonified by the acoustic signals emitted by the Heard Island sound source. Using numerical models it was demonstrated that reliable, unimpeded acoustic paths over cross-basin ranges do exist. The expected arrival positions of

reliable rays launched at Heard Island fluctuate between 34.56°N / 239.55°E and 37.02°N / 237.58°E, roughly from San Francisco to Santa Barbara on the California coast, with a mean focus at 36.06°N / 238.36°E. This suggests that a receiver array should optimally be located at, or close to, this position. Standard deviations of the envelope foci were about 0.25° and the centers of the insonification envelopes in general do not coincide with these foci. The average strength of the focal points, as expressed by the envelope divergences, was 58.7 km, but with large variability.

Ray arrivals near the Oregon coast are possible, but have a less reliable nature. Frequent bottom interactions in the relatively shallow Tasman Sea will deplete the acoustic energy of these rays so much that it will be hard, if not impossible, to detect the corresponding arrivals.

3. Wave Front Travel Time Variability

Estimated wave front travel times are on the order of 12060 s, although it was shown that spatial variations within an envelope can be as large as 131 s, depending on the envelope width. Estimated temporal rms fluctuations have a magnitude of about ± 15 s.

An important finding is that a clear distinction can be made between two types of rays with different characteristics. All rays that were

72

examined fell into either one of these categories. Type I rays, which are trapped close to the surface up to approximately 8000 km ranges and exhibit a large ray amplitude away from the transition zone, were shown to arrive earlier than Type II rays. Rays of the latter type enter the deep sound channel sooner, at ranges of about 5000 km and will have a much smaller ray amplitude away from the transition zone. Consequently, wave front travel times for this type of rays are longer than for the Type I rays. Temporal variability was found to be larger for the Type I rays than for the Type II rays. This is due to the fact that Type I rays traverse larger distances away from the sound channel axis, partly through the oceanic thermocline, where sound speed fluctuations are expected to be more pronounced. Type II rays are confined much closer to the axis, away from the thermocline. Because of lesser contamination by the meso- and gyre scale variability Type II rays appear to be better suited for the detection of climate change in the deep ocean. However, only Type I rays contain information about ocean temperature fluctuations in the upper part of the water column.

4. Azimuthal Arrival Angles

Estimated azimuthal arrival angles vary between approximately 33.7° and 45.0°, with an average of about 39.0°. A permanent (horizontal)

receiver array should optimally be oriented in a direction close to this average. Expected temporal rms fluctuations in arrival angles are on the order of $\pm$ 4.0°. An optimal receiver beam-width should be on the same order of magnitude.

5. Shallow Seamounts

It was found that the shallow Fieberling and Erben seamounts, close to the California coast, will not impede the acoustic transmissions. Both are located well to the north of the incoming acoustic rays.

6. Interfacing Procedure

To aid in the continuous effort to examine whether existing ocean/acoustic interfacing procedures and methods in ongoing acoustic computer simulation studies can be improved upon in terms of accuracy and efficiency, two alternative methods to interpolate gridded sound speed data were examined. The results indicate that the EOF method developed by Newhall, et al. (1986) is better suited for this kind of study.

7. Naval Operations

In the context of antisubmarine warfare operations an important finding is that reliable acoustic paths over cross-basin ranges can exist. Depending on source levels and frequencies, detection of submarines over such long ranges might be possible. Furthermore it was shown how

several important acoustic parameters are expected to vary under the influence of ocean m~so- and gyre scale ocean variability This knowledge about the variability in space and time of the acoustic wave fields that propagate through oceanic fronts and eddies may aid in future design and use of sonar and in the interpretation of the results in an operational setup. Finally, this thesis has demonstrated the feasibility of coupling global oceanic and acoustic models. Such integration can be applied to future on-board, long range acoustic propagation prediction systems in support of antisubmarine warfare operations.

B. FINAL REMARKS AND RECOMMENDATIONS

In this last section some final comments will be made. The scope and methods of the research imposed some limitations, which must be kept in mind when looking at the results.

First, only a limited number of rays (generally about seven) were traced for each of the ocean model output data fields. The fact that the raytracing had to be carried out in a small UNIX workstation environment, in which each raytracing run took about 12-14 wall-clock hours, limited the number of runs that could be carried out in the available time. Results produced by applying statistical formulas, that inherently assume large samples, therefore only represent rough "estimates". This thesis

should thus be viewed as an initial investigation, which must be expanded in the future. Carrying out a large number of additional raytracing runs, could greatly enhance the statistical significance of the results. Future availability of a supercomputer, on which these additional runs can be carried out simultaneously in a shorter time frame, is highly desirable for this kind of study.

Whether the temporal variability in wave front travel times will or will not allow detection of the expected greenhouse signal in a permanent global climate monitoring system, depends on whether this variability can be reduced through averaging. Significantly more raytracing runs, to produce a long time series, could be helpful in solving this problem.

Secondly, it was shown that rays are very sensitive to small variations in the sound speed structure. This is partly due to the fact that geometric raytracing is a high frequency approximation. To complement the results presented here and to aid in interpreting them, analyses using alternative techniques that take into account the finite frequency effects, such as dispersion and diffraction, will be necessary[4].

Thirdly, ocean currents were ignored in the setup of the analysis. The cumulative effects of currents are not necessarily insignificant, due to the

---

4 Examples of such "full-wave" methods are normal mode and parabolic equation analyses

very long path length under consideration. The same is true for seasonal effects. The ocean model output data sets used here, were obtained from model runs with seasonally constant forcing[5]. Future investigations should incorporate ocean currents, as well as seasonal forcing, to quantify the effects on the acoustic parameters discussed in this thesis.

Another limiting factor results from the fact that the grid resolution of the Semtner-Chervin global ocean general circulation model is just marginally enough to resolve mesoscale eddies and fronts. When the next generation of supercomputers becomes available, the grid resolution should be increased to resolve smaller scale ocean fluctuations. Future acoustic simulations can then assess the impact of this smaller scale variability by using model output data fields with the enhanced grid resolution.

Also, it was noted that this analysis did not allow for geodesic veering of acoustic rays under the influence of the earth's ellipticity. Future investigations should incorporate ellipticity corrections in the raytracing code.

---

[5] Recently seasonal forcing was incorporated in the ocean model. Output over ten model years, extracted at 3 day simulation time interval, is presently available at the National Center for Atmospheric Research (Semtner, 1990)

REFERENCES

Altman, D., NorthWest Research Associates Inc., Bellevue, Washington, personal communication, 1990.

Barnett, T., and M. Schlesinger, 1988: Detecting Changes in Global Climate Induced by Greenhouse Gases., *J. Geophys. Res.*, **92**, 14772-14780.

Bryan, K., and M.D. Cox, 1967: A Numerical Investigation of the Oceanic General Circulation., *Tellus*, **XIX**, 54-80.

Chen, C.T., and F.J. Millero, 1977: Speed of Sound in Seawater at High Pressures., *J. Acoustic. Soc. Am.*, **62** 1129-1135.

Chervin, R.M., 1990: High Performance Computing and the Grand Challenge of Climate Modeling., *Comp. in Phys.*, **Special Issue, May/June**, 234-239.

Chiu, C.S, and L.L. Ehret, 1990: Computations of Sound Propagation in a Three-dimensionally Varying Ocean: A Coupled Normal Mode Approach. *Comp. Acoustics*, **1**, 187-202.

Chiu, C.S, A.J. Semtner and L.L. Ehret, 1990: *Computer Simulation Studies of Low-frequency Cross-basin Acoustic Transmissions*, Progress Report to the Office of Naval Research, 15 pp.

Ehret, L.L., Code EC/Eh, Department of Electrical and Computer Engineering, Naval Postgraduate School, Monterey. California, personal communication, 1990.

Franke R., 1979: *A Critical Comparison of Some Methods for Interpolation of Scattered Data*, Technical Report NPS-53-79-003, Naval Postgraduate School, Monterey, California, 373 pp.

Hardy, R.L., 1990: Theory and Applications of the Multiquadric-Biharmonic Method; 20 years of discovery 1968-1988., *Comp. Math. Applic.*, **19**, 163-208.

Hellerman, S., and M. Rosenstein, 1983: Normal Monthly Wind Stress over the World Ocean with Error Estimates., *J. Phys. Oceanogr.*, **13**, 1093-1104.

Jones, Ph.D., and T.M.L. Wigley, 1990: Global Warming Trends., *Sci. Am.*, **263**, 84-91.

Jones, R.M., J.P. Riley and T.M. Georges, 1986: HARPO a Versatile Three-Dimensional Hamiltonian Ray-tracing Program for Acoustic Waves in an Ocean with Irregular Bottom., *Wave Prop. Lab. NOAA*, Boulder, Colorado, 457 pp.

Kansa, E.J., 1990: Multiquadrics - A Scattered Data Approximation Scheme With Applications to Computational Fluid Dynamics - I ; Surface Approximations and Partial Derivative Estimates., *Comp. Math. Applic.*, **19**, 127-145.

Levitus, S., 1982: Climatological Atlas of the World Oceans., *NOAA Prof. Pap. 13*, U.S. Government Printing Office, Washington D.C.

Lighthill, J. 1987: *Waves in Fluids*, Cambridge University Press, Great Britain, 504 pp.

Long, E.C., 1990: *Analysis of an Eddy-Resolving Global Ocean Model in the Tropical Indian Ocean.*, M.S. thesis, Department of Oceanography, U.S. Naval Postgraduate School, Monterey, 147 pp.

Mackenzie, K.V., 1981: Nine-term Equation for Sound Speed in the Oceans., *J. Acoustic. Soc. Am.*, **70**, 807-812.

Munk, W.H., and A.M.G. Forbes, 1989: Global Ocean Warming: An Acoustic Measure?, *J. Phys. Oceanogr.*, **19**,1765-1778.

Newhall, A.E., J.F. Lynch, C.S. Chiu and J.R. Daugherty, 1989: Improvements in Three-dimensional Raytracing Codes for Underwater Acoustics., *MIT/WHOI Joint Program Woods Hole, MA 02543*, 29 pp.

Semtner, A.J., Code OC/Se, Department of Oceanography Naval Postgraduate School, Monterey, California, personal communication, 1990.

Semtner, A.J., and R.M. Chervin, 1988: A Simulation of the Global Ocean Circulation with Resolved Eddies., *J. Geophys. Res.*, **93**, 15502-15522.

Semtner, A.J., and R.M. Chervin, 1990: Environmental Effects on Acoustic Measures of Global Ocean Warming., *J. Geophys. Res.*, **95**, 12973-12982.

Shockley, R.C., J. Northrop, P.G. Hansen, and C. Hartdegen, 1982: SOFAR Propagation Paths from Australia to Bermuda: Comparison of Signal Speed Algorithms and Experiments., *J. Acoust. Soc. Am.*, **71**, 51-60.

Spindel, R.C., 1985: Signal Processing in Ocean Tomography., *Adaptive Methods in Underwater Acoustics*, H.G. Urban, Ed., D. Reidel Publishing Company, 687-710.

INITIAL DISTRIBUTION LIST

		No. Copies
1.	Defense Technical Information Center Cameron Station Alexandria, VA 22304-6145	2
2.	Library, Code 52 Naval Postgraduate School Monterey, CA 93943-5002	2
3.	Chairman (Code OC/Co) Department of Oceanography Naval Postgraduate School Monterey, CA 93943-5000	1
4.	Chairman (Code MR/Hy) Department of Meteorology Naval Postgraduate School Monterey, CA 93943-5000	1
5.	The Hydrographer of the Royal Netherlands Navy Bureau Hydrografie Badhuisweg 171 2597 JN Den Haag The Netherlands	3
6.	Professor C.S. Chiu, (Code OC/Ci) Department of Oceanography Naval Postgraduate School Monterey, CA 93943-5000	5
7.	Professor A.J. Semtner, (Code OC/Se) Department of Oceanography Naval Postgraduate School Monterey, CA 93943-5000	1